MOLECULAR NONLINEAR OPTICS
(ACADEMIC PRESS, NEW YORK)
J. ZYSS, ED. (1994)

Chapter 1

MANY-BODY EFFECTS IN NONLINEAR SUSCEPTIBILITIES; BEYOND THE LOCAL-FIELD APPROXIMATION

Shaul Mukamel

Department of Chemistry, University of Rochester, Rochester, New York

1. INTRODUCTION

The systematic calculation of nonlinear susceptibilities of optical materials, and the precise relationship between individual molecular hyperpolarizablities and the macroscopic optical response, constitute a complex challenge that has drawn a considerable theoretical attention [1–5]. The design of new optical materials with specified characteristics (fast switching, large susceptibilities) and the interpretation of nonlinear optical measurements in terms of molecular properties and intermolecular forces require the development of a suitable theoretical framework.

The response of a medium to optical fields is most conveniently formulated in terms of wave vector and frequency-dependent optical susceptibilities, which are the expansion coefficients of the macroscopic polarization field in powers of the Maxwell electric field E [6–9]. The problem of incorporating intermolecular forces in the linear optical response (i.e., the dielectric function) has a long history [10–15]. The local-field approximation provides a simple way to relate the polarizabilities of isolated molecules to the macroscopic susceptibilities. In this approach, the effect of intermolecular forces is included in an effective local electric field. The problem of calculating the response of an interacting ensemble of molecules to the electromagnetic field is then reduced to the response of isolated molecules interacting with the local field $\mathbf{E}_L$, through an interaction Hamiltonian $-\boldsymbol{\mu}\cdot\mathbf{E}_L$, where $\boldsymbol{\mu}$ denotes the molecular dipole operator. The Lorentz relation between the local field and the Maxwell field $\mathbf{E}$ (Eq. 1.4.2) can then be used to calculate the dielectric function. This procedure, which reduces the complex many-body problem to a single-body problem, was subsequently generalized and applied also to the calculation of nonlinear susceptibilities [3,5,9,16–18]. The nonlinear susceptibilities at a given order are then given in terms of sums of products of molecular polarizabilities of that order and lower orders. This simple, back-of-the-envelope calculation of macroscopic susceptibilities is, however, not rigorous [5,19]. It fails to take properly into account the correlated dynamics of the interacting many-body system, i.e. correlations among the molecules, as well as correlations between the molecules and the radiation field. Short-range (e.g., exchange) forces are totally neglected in this procedure. Moreover, even the dipole–dipole forces are not fully taken into account. In addition, the resulting susceptibilities do not depend on the wavevectors, apart from the local-field contribution, but just on the frequencies. This indicates that processes such as exciton migration and energy transfer and transport (e.g., the Forster transfer) [20,21] are neglected. Such processes are often added phenomenologically in order to interpret transient

grating spectroscopy [22,23], which is a four-wave mixing technique that measures transport processes by following the wave vector dependence of the susceptibilities. The common derivation of the local-field approximation [3] cannot be extended to include these processes, since it is intrinsically a mean-field single-molecule theory.

Moreover, the local-field approximation totally misses any collective effects resulting from cooperative interactions with the radiation field. Such effects are particularly important in the studies of optical nonlinearities of molecular [24–29] and semiconductor [4,30–36] systems with restricted geometries. Such studies are currently drawing considerable attention, due to the significant progress made in the fabrication of nanostructures such as microcrystallites, monolayers and quantum wires. Quantum well structures in semiconductors show sharp exciton resonances even at room temperature, and their nonlinear optical properties have been studied extensively [35]. One of the most fascinating open questions raised by these studies is the possibility of maintaining a large coherence size [28,29] which may give rise to enhanced nonlinear optical susceptibilities and ultrafast radiative decay rates [30,37,38], which result from collective (cooperative) interactions with the radiation field. These effects are totally absent in the local-field level of description since they involve explicitly intermolecular (non-local) coherences. Simple back-of-the-envelope argument [27] suggests that the transition dipole matrix element in an aggregate with N molecules should scale as $\sim\sqrt{N}$. $\chi^{(3)}$, which is proportional to the dipole moment to the fourth power, should therefore scale as $\sim N^2$, whereas if the molecules were independent it would scale as $\sim N$. We thus expect an extra N enhancement of $\chi^{(3)}$ upon aggregation. This argument was shown to be misleading [28,29]. Interference effects cancel this enhancement under off-resonant conditions. The resonant enhancement is expected to saturate with aggregate size [28]. The interaction with a thermal bath introduces fluctuations [39] that result in intermolecular dephasing and inhomogeneous broadening, which may destroy the coherence among different molecules. We expect that due to the dephasing processes, N should be replaced by N_{eff} where $N_{\text{eff}} < N$ is the effective number of coherently coupled molecules. N_{eff} is expected to attain the limiting value $N_{\text{eff}} = 1$ as the dephasing rate becomes sufficiently large to decouple the radiative dynamics of the various molecules. It is clear from the above arguments that the main problem in predicting the nonlinear optical response of optical materials is not how to better calculate the local field, but rather the fundamental failure of the local-field approximation to describe and predict some very important effects related to the many-body nature of the problem. A new theoretical approach is called for that goes beyond the local-field approximation.

In this review we present a microscopic theoretical framework for the calculation of the nonlinear optical response of molecular materials with localized electronic states that accounts for intermolecular interactions and dynamic correlations and overcomes the difficulties associated with the local-field approach. The present theory is based on the derivation of coupled reduced equations of motion for the material variables, which determine the optical response [5,19,28,39]. We find that in addition to the single-particle variables, we need consider also two-exciton and exciton-population variables which represent intermolecular coherences. The material system can thus be modelled as a collection of coupled anharmonic oscillators. An anharmonic oscillator picture of the nonlinear response has been suggested as a qualitative model [6,9,40] since the early days of nonlinear optics. The equation of motion approach [5,36] shows how such a picture can be rigorously established and applied toward the fully microscopic determination of the coherence size [28,36]. The effects of various factors (size, temperature, geometry, and exciton-phonon coupling) on the cooperative can be studied.

Many practical applications of optical material use laser frequencies that are far detuned from any molecular resonant frequency (electronic or vibrational). This is done to avoid absorption and other competing processes and to obtain faster switching timescales. Spectroscopic applications of nonlinear optics, on the other hand, often use resonant frequencies that provide a direct probe for specific energy levels and their dynamics [9,41,42]. We shall explore the nonlinear susceptibilities in both regimes. We show that for parametric (off-resonant) processes, cooperative effects will not be of great significance, but as some of the frequencies in the process are tuned near resonance, they may play an important role. Comparison with resonant spectroscopic measurements should establish the validity of the approximations made in the theory and allow us to predict with confidence the off-resonant optical response. For the sake of clarity we shall not consider here cooperative spontaneous emission (superradiance) [37,43–45] whose coherence size is closely related to that of optical nonlinearities. Polariton effects, which are important in materials with a large oscillator strength per unit volume at low temperatures [46–50] and require the incorporation of retarded interactions and a quantum description of the radiation field, were reviewed recently [5] and will not be discussed here.

In Sec. 2 we introduce the model system of a molecular crystal with Frenkel excitons. The basic equations of motion with intermolecular interactions are derived in Sec. 3. In Sec. 4 we present the single-particle level and in Sec. 5 we investigate the role of two-exciton variables in the enhancement of nonlinear susceptibilities in molecular aggregates. The role of exciton-population variables that are the source of intramolecular nonlinearities (known in the semiconductor literature as "phase-space filling") is investigated in Sec. 6. We further explore the effects of exciton transport using the Wigner phase-space distribution. In Sec. 7 we combine all bilinear exciton variables and present general equations of motion and a Green function expression for $\chi^{(3)}$. We analyze the nonlinear coherence size and discuss the limitations of the local-field approximation. In Sec. 8 we summarize our results.

2. MODEL HAMILTONIAN FOR MOLECULAR MATERIALS; FRENKEL-EXCITONS

In order to explore the role of many-body effects in the macroscopic nonlinear optical response, we consider a model system consisting of a lattice of polarizable (nonpolar) two-level molecules with transition frequency Ω and one molecule per unit cell [11,51,52]. In the dipole approximation, the Hamiltonian for our system is [5]:

$$H = H_{\text{mat}} - \int P(\mathbf{r}) \cdot E(\mathbf{r}, t) d\mathbf{r}. \tag{1.2.1}$$

Here, H_{mat} denotes the material Hamiltonian which can be partitioned as follows:

$$H_{\text{mat}} = H_{\text{ex}} + H_{\text{ph}} + H_{\text{ep}}. \tag{1.2.2a}$$

H_{ex} is the Frenkel-exciton Hamiltonian

$$H_{\text{ex}} = \hbar\Omega \sum_m B_m^\dagger B_m + \frac{\hbar}{2} \sum_{m,n}{}' J(\mathbf{r}_{mn})(B_m^\dagger + B_m)(B_n^\dagger + B_n), \tag{1.2.2b}$$

$B_m^\dagger$ (B_m) denotes the creation (annihilation) operator for an excitation on molecule m with transition frequency Ω. These operators commute for different molecules, whereas for any single molecule they obey the Pauli anticommutation relation

$$B_m^\dagger B_m + B_m B_m^\dagger = 1. \tag{1.2.3}$$

Equation (1.2.3) can alternatively be written in the form $[B_m, B_m^\dagger] = 1 - W_m$ with the exciton population operator $W_m \equiv 2B_m^\dagger B_m$. For harmonic oscillators (bosons), Eq. (1.2.3) does not hold and $[B_m, B_m^\dagger] = 1$. Therefore, neglecting the W_m operator for two-level molecules is usually denoted the Bose approximation. We note that in the present model the Pauli exclusion is the only source of nonlinearities. In systems with multilevel (and polar two level)

molecules, other sources arise from intermolecular interaction terms that are cubic and quartic in the molecular exciton creation and annihilation operators [21,53]. Such terms give rise to nonlinearities even if a Bose approximation is applied. The second term in H_{ex} accounts for the instantaneous dipole–dipole interactions between the molecules in their equilibrium positions and orientations (the prime excludes terms with $m = n$ from the summation),

$$\hbar J(\mathbf{r}) = \tilde{\mu}\cdot\left(\frac{1}{\mathbf{r}^3} - \frac{3\mathbf{r}\mathbf{r}}{\mathbf{r}^5}\right)\cdot\tilde{\mu}. \tag{1.2.4}$$

Here $\mathbf{r}_{mn} \equiv \mathbf{r}_m - \mathbf{r}_n$, where $\mathbf{r}_m$ denotes the equilibrium position of molecule m, with $\tilde{\mu}$ denoting the molecular transition dipole in the equilibrium configuration (equal for all molecules on the lattice). In the present model the excitons have therefore two types of interaction: the dipole–dipole interaction and the Pauli exclusion which can effectively be viewed as a repulsive interaction.

The second contribution to H_{mat}, H_{ph}, represents the nuclear (phonon) motions and the last contribution to H_{mat} is the exciton–phonon interaction, which arises from the dependence of the intermolecular interactions on the displacements of the nuclear coordinates from their equilibrium values. The coupling with phonons plays an important role in determining the coherence size and the magnitude of optical nonlinearities. For the sake of clarity we shall use here simplified models for the exciton–phonon coupling, although a more rigorous treatment of this coupling may be carried out [5.51].

The second term in H represents the coupling to a classical transverse electric field $E(\mathbf{r})$. $P(\mathbf{r})$ is the optical polarization operator, which may be written as

$$P(\mathbf{r}) = \sum_m \tilde{\mu}(B_m + B_m^\dagger)\delta(\mathbf{r} - \mathbf{r}_m), \tag{1.2.5}$$

where we assumed that all molecular transition dipole matrix elements are parallel and given by $\tilde{\mu}$. We shall further introduce the material polarization field in momentum space

$$P(\mathbf{k}) \equiv \sqrt{N}\,\tilde{\mu}(B_{\mathbf{k}} + B^\dagger_{-\mathbf{k}}), \tag{1.2.6}$$

where we have defined the exciton annihilation $B_{\mathbf{k}}$ and creation $B^\dagger_{-\mathbf{k}}$ operators in the momentum representation

$$B_{\mathbf{k}} \equiv \frac{1}{\sqrt{N}}\sum_m B_m \exp(i\mathbf{k}\cdot\mathbf{r}_m), \tag{1.2.7a}$$

$$B^\dagger_{-\mathbf{k}} \equiv \frac{1}{\sqrt{N}}\sum_m B_m^\dagger \exp(i\mathbf{k}\cdot\mathbf{r}_m). \tag{1.2.7b}$$

3. EQUATIONS OF MOTION: THE ANHARMONIC-OSCILLATORS PICTURE

Nonlinear susceptibilities of simple quantum systems are usually calculated using the time-dependent density matrix (the Schrödinger picture) [6–9]. The susceptibilities are then given in terms of multiple summations over eigenstates. In order to map the problem into coupled anharmonic oscillators, we adopt in the present work a different route, which is based on the Heisenberg picture. The polarization will be calculated by solving a set of coupled nonlinear equations of motion. The equations are obtained by identifying a set of relevant dynamical variables and deriving equations of motion for their expectation values [5,28,36]. Our starting point is the Heisenberg equation of motion for any material operator A

$$\dot{A} = \frac{i}{\hbar}[H, A]. \tag{1.3.1}$$

Since the polarization operator is expressed in terms of B_n and $B_n^\dagger$, it is natural to start with the equations of motion for these operators. Using the Hamiltonian Eq. (1.2.1) and the commutation relation (1.2.3), we obtain the following equations of motion (all operators taken at time t):

$$\frac{1}{i}\frac{d}{dt}B_n = -\Omega B_n - \sum_m{}' (J_{nm} - i\Gamma_{nm})B_m - \sum_m J_{nm}B_m^\dagger$$
$$+ 2\sum_m{}' J_{nm}(B_n^\dagger B_n B_m + B_n^\dagger B_n B_m^\dagger) + \frac{1}{\hbar}\tilde{\mu}\cdot E(\mathbf{r}_n, t)[1 - 2B_n^\dagger B_n]. \tag{1.3.2}$$

Equation (1.3.2) is the basis for all the equations of motion derived here. Γ_{nm} is an exciton relaxation term which is introduced here phenomenologically. The first three terms in the r.h.s. of Eq. (1.3.2) represent linear dynamics whereby B_n is coupled to B_m and $B_m^\dagger$. The other two terms are more complex. They represent nonlinear coupling to higher order operators $B_n^\dagger B_n$, $B_n^\dagger B_n B_m$ and $B_n^\dagger B_n B_m^\dagger$. Equation (1.3.2) is therefore not closed. We may proceed by taking $A = B_n^\dagger B_n$, $B_n^\dagger B_n B_m$, and $B_n^\dagger B_n B_m^\dagger$ and writing the Heisenberg equations for these operators. We shall then couple them to even more complex operators involving products of four B operators. In general, Eq. (1.3.1) will therefore result in an infinite hierarchy of coupled dynamical equations whereby single-body operators are successively coupled to more complex operators. Fortunately, the optical response to electromagnetic fields that are not too strong requires the explicit introduction of only few-particle states. This allows us to truncate the hierarchy at a very early

stage. The main problem addressed in this review is the possible truncation schemes that yield a hierarchy of approximations for the nonlinear optical response. We shall demonstrate how a truncation at the two-particle level may be adequate for the calculation of a variety of optical measurements. This situation is formally very similar to zero-temperature many-body theory where a few quasiparticles dominate the dynamical behavior [54].

Let us first consider the linearized part of Eq. (1.3.2) by neglecting the last two terms, which represent nonlinear dynamics and the driving field. By considering an infinite periodic structure and switching to k-space, the equation reads

$$\frac{1}{i}\frac{d}{dt}B_{\mathbf{k}} = [-\Omega - J(\mathbf{k}) + i\Gamma(\mathbf{k}]B_{\mathbf{k}} - J(\mathbf{k})B^{\dagger}_{-\mathbf{k}}. \tag{1.3.3}$$

Here, $J(\mathbf{k})$ is the lattice Fourier transform of the intermolecular interaction

$$J(\mathbf{k}) = \sum_{m\neq 0} J(\mathbf{r}_m)\exp(-i\mathbf{k}\cdot\mathbf{r}_m). \tag{1.3.4}$$

For a centrosymmetric lattice, we have $J(\mathbf{k}) = J(-\mathbf{k})$. $\Gamma(\mathbf{k})$ is the damping rate of the exciton induced by the phonon bath. Equation (1.3.3), together with its Hermitian conjugate equation for $B^{\dagger}_{-\mathbf{k}}$, defines an eigenvalue problem whose solutions are the creation and annihilation operators for the Coulomb exciton at wave vector $\mathbf{k}$ in terms of $B_{\mathbf{k}}$ and $B^{\dagger}_{-\mathbf{k}}$. The Coulomb exciton frequency is determined by the secular equation of the problem and easily found to be $\Omega_{\mathbf{k}} - i\Gamma(\mathbf{k})$, with

$$\Omega_{\mathbf{k}} = [\Omega(\Omega + 2J(\mathbf{k}))]^{1/2}. \tag{1.3.5}$$

For $|J(\mathbf{k})| \ll \Omega$, which is by definition the case in molecular crystals [51], this yields $\Omega_{\mathbf{k}} \approx \Omega + J(\mathbf{k})$. This is known as the Heitler-London approximation whereby the Coulomb excitons are simply created (annihilated) by $B^{\dagger}_{-\mathbf{k}}$ ($B_{\mathbf{k}}$).

We now discuss the linear optical response, which is governed by the first-order susceptibility. To that end we define the discrete Fourier decomposition of the field,

$$\mathbf{E}(\mathbf{r}, t) = \sum_j [\mathbf{E}_j \exp(i\mathbf{k}_j\cdot\mathbf{r} - i\omega_j t) + c.c.], \tag{1.3.6}$$

where j labels a few modes that are relevant in the experiment. ω_j (>0) and $\mathbf{k}_j$ are related by the crystal's dispersion relation. Similar decomposition is possible for the polarization field $\mathbf{P}(\mathbf{r}, t)$. The susceptibilities are defined as the coefficients appearing in the expansion of the amplitudes $\mathbf{P}_j$ in terms

of powers of the electric field amplitudes $\mathbf{E}_j$. The first order susceptibility is easily obtained from Eq. (1.3.2). The part of the polarization that is linear in the electric field is found by neglecting the nonlinearities (the $B^{\dagger}_n B_n B_m$, $B^{\dagger}_n B_n B^{\dagger}_m$ and the $B^{\dagger}_n B_m$ terms). After taking expectation values and substituting Eq. (1.3.6) and its analog for the polarization, we obtain

$$\mathbf{P}^{(1)}_j \equiv \chi^{(1)}(\mathbf{k}_j, \omega_j)\cdot\mathbf{E}_j, \tag{1.3.7a}$$

with the linear susceptibility tensor $\chi^{(1)}(\mathbf{k}, \omega) \equiv (\varepsilon(\mathbf{k}, \omega) - 1)/4\pi$, $\varepsilon(\mathbf{k}, \omega)$ being the frequency and wave vector dependent dielectric tensor. We finally get [11,46]

$$\varepsilon(\mathbf{k}, \omega) = 1 + \frac{8\pi\Omega\rho\hbar^{-1}\tilde{\mu}\tilde{\mu}}{-[\omega + i\Gamma(\mathbf{k})]^2 + \Omega^2_{\mathbf{k}}}, \tag{1.3.7b}$$

where $\rho \equiv N/V$ denotes the average molecular density in the crystal, and the superscripts in parentheses indicate the order in the electric field amplitudes.

We next turn to the calculation of optical nonlinearities. We note that $\chi^{(3)}$ is the lowest nonlinearity allowed by the present model, since $\chi^{(2)}$ vanishes for a centrosymmetric medium [6]. $\chi^{(3)}$ in general represents a broad class of processes known as four-wave mixing. In a frequency-domain four-wave mixing experiment we consider three fundamental fields ($j = 1, 2, 3$ in Eq. 1.3.6) and are interested in the signal at $(\mathbf{k}_s, \omega_s) \equiv (\mathbf{k}_1 - \mathbf{k}_2 + \mathbf{k}_3, \omega_1 - \omega_2 + \omega_3)$. To lowest order in the field amplitudes $\mathbf{E}_j$ this is determined by the third order susceptibility, which is defined through

$$\mathbf{P}^{(3)}_s \equiv \chi^{(3)}(-\mathbf{k}_s - \omega_s; \mathbf{k}_1\omega_1, -\mathbf{k}_2 - \omega_2, \mathbf{k}_3\omega_3)\mathbf{E}_1\mathbf{E}^{*}_2\mathbf{E}_3, \tag{1.3.8}$$

where $\mathbf{P}^{(3)}_s$ is the discrete Fourier coefficient of the polarization field with wave vector $\mathbf{k}_s \equiv \mathbf{k}_1 - \mathbf{k}_2 + \mathbf{k}_3$ and frequency $\omega_s \equiv \omega_1 - \omega_2 + \omega_3$ to third order in the electric field amplitudes. Other choices of $\mathbf{k}_s$ and ω_s can be obtained by changing the signs of one or more ω_j and $\mathbf{k}_j$ variables. When the expectation value of Eq. (1.3.2) is taken, we find that the single-particle variables $\langle B^{\dagger}_n\rangle$ are coupled to the two-operator variables $\langle B^{\dagger}_n B_n\rangle$ and to the three operator (two-particle) variables $\langle B^{\dagger}_n B_n B_m\rangle$ and $\langle B^{\dagger}_n B_n B^{\dagger}_m\rangle$. In most calculations presented in this article, we shall invoke the Heitler-London approximation, thereby neglecting certain off-resonant contributions to the nonlinear response. This amounts to neglecting the $B^{\dagger}_n$ and the $B^{\dagger}_n B_n B^{\dagger}_m$ terms in the r.h.s. of Eq. (1.3.2). In the discussion below we shall therefore not consider the $\langle B^{\dagger}_n B_n B^{\dagger}_m\rangle$ variables, although they may be treated very similarly to the $\langle B^{\dagger}_n B_n B_m\rangle$ variables (see Eq. (1.7.1).

The $\langle B^{\dagger}_n B_n\rangle$ variables represent exciton populations, and they are the source of nonlinearity in the single-particle formulation of nonlinear optics,

which is based on the Bloch equations. In the semiconductor literature this contribution is known as "phase space filling" [35]. These single-particle variables pose no major theoretical problem; the story is very different for the $\langle B_n^\dagger B_n B_m\rangle$ terms. The rigorous way to proceed is to derive an equation of motion for $\langle B_n^\dagger B_n B_m\rangle$ which, when solved coupled with $\langle B_n^\dagger\rangle$ and $\langle B_n\rangle$, will yield the nonlinear response. It is important to recognize that all existing theories for the nonlinear optical response contain an (either implicit or explicit) approximation for these three-operator quantities. In this review we present a systematic approach and discuss the hierarchy of possible approximations. To gain some insight into the issue, it proves useful to switch for a moment to the Schrödinger picture and describe the system using the density matrix $\rho(t)$. It should be emphasized that eventually we are going to derive and solve equations of motion for the expectation values of dynamical variables; we are not going to calculate the density matrix. We use the density matrix here only in order to clarify the physical significance of the various factorizations. In the Schrödinger picture we have

$$\langle B_n^\dagger(t)B_n(t)B_m(t)\rangle \equiv Tr[B_n^\dagger(0)B_n(0)B_m(0)\rho(t)] \tag{1.3.9}$$

(where the time argument is explicitly indicated). Here

$$B_n(t) \equiv \exp(iH_{\text{mat}}t)B_n \exp(-iH_{\text{mat}}t)$$

are the operators in the Heisenberg picture and

$$\rho(t) \equiv \exp(-iH_{\text{mat}}t)\rho(0)\exp(iH_{\text{mat}}t)$$

is the density matrix in the Schrödinger picture. By introducing an ansatz for $\rho(t)$ it is possible to express Eq. (1.3.9) using lower order operators and thus close to hierarchy. In the coming sections we shall explore the following approximations for the three-operator quantities.

1. *Single-Particle Factorization.* The single-particle factorization is introduced in Sec. 4, where we set
$$\langle B_n^\dagger B_n B_m\rangle = \langle B_n^\dagger\rangle\langle B_n\rangle\langle B_m\rangle. \tag{1.3.10}$$
This is the simplest possible truncation of the hierarchy, since it retains only the exciton amplitude variables.
2. *Factorization into Two-Exciton Variables.* Neglecting phonons, the density matrix of the system represents a pure state $\rho(t) = |\psi(t)\rangle\langle\psi(t)|$, where $\psi(t)$ is the wave function. In this case we can rigorously factorize the creation and the annihilation operators in the calculation of $\chi^{(3)}$. [28]
$$\langle B_n^\dagger B_n B_m\rangle = \langle B_n^\dagger\rangle\langle B_n B_m\rangle. \tag{1.3.11}$$

The $\langle B_n B_m\rangle$ variables represent two-exciton dynamics. This level of the hierarchy will be discussed in Sec. 5.

3. *Factorization into Exciton-Population Variables.* Neglecting all correlations among different sites we set for $n \neq m$ [5,55]
$$\langle B_n^\dagger B_n B_m\rangle = \langle B_n^\dagger B_n\rangle\langle B_m\rangle. \tag{1.3.12}$$
The $\langle B_n^\dagger B_n\rangle$ variables represent exciton populations, and their dynamics may be related to standard transport equations (the Boltzmann and the diffusion equations). This level of the hierarchy will be discussed in Sec. 6.
4. *Inclusion of Two-Exciton and Exciton-Population Variables.* A more general factorization which includes the previous factorizations as special cases is
$$\langle B_n^\dagger B_n B_m\rangle = \langle B_n^\dagger B_n\rangle\langle B_m\rangle + \langle B_n^\dagger B_m\rangle\langle B_n\rangle + \langle B_n^\dagger\rangle\langle B_n B_m\rangle - 2\langle B_n^\dagger\rangle\langle B_n\rangle\langle B_m\rangle. \tag{1.3.13}$$
Equation (1.3.13) may be derived using an approximation maximum-entropy form for the density matrix $\rho(t)$ [39]. When Eq. (1.3.13) is used without introducing any further factorization, we incorporate all exciton populations ($\langle B_n^\dagger B_n\rangle$), exciton-coherence ($\langle B_n^\dagger B_m\rangle$), and two-exciton ($\langle B_n B_n\rangle$) variables. These variables, together with the single-exciton ($\langle B_n\rangle$) variables and their Hermitian conjugates, constitute the complete set of binary dynamical variables. Equation (1.3.13) will be discussed in Sec. 7. As indicated earlier, cases 1 to 3 are special cases of (4). Starting with Eq. (1.3.13), if we further factorize all operators, or creation and annihilation operators, or operators belonging to different sites, we recover Eqs. (1.3.10), (1.3.11), and (1.3.12) respectively.

4. THE SINGLE-PARTICLE LEVEL AND THE LOCAL-FIELD APPROXIMATION

The simplest approximation for the nonlinear response is obtained by adopting the single-particle factorization (Eq. 1.3.10). Taking the expectation value of Eq. (1.3.2) and its hermitian conjugate, substituting $\langle B_n^\dagger B_n B_m\rangle = \langle B_n^\dagger\rangle\langle B_n\rangle\langle B_m\rangle$ and $\langle B_n^\dagger B_n\rangle = \langle B_n^\dagger\rangle\langle B_n\rangle$, and using the definition of the polarization (Eq. 1.2.5), we finally get a closed equation for the polarization [5].

$$\ddot{P}(\mathbf{r},t) + 2\Gamma\dot{P}(\mathbf{r},t) + \Omega^2 P(\mathbf{r},t) = 2\Omega\rho\hbar^{-1}|\mu|^2\cdot\mathbf{E}_L(\mathbf{r},t) - \frac{1}{\hbar\Omega\rho}\mathbf{E}_L; j(\mathbf{r},t)|(\Omega + i\Gamma)P(\mathbf{r},t) + i\dot{P}(\mathbf{r},t)|^2. \tag{1.4.1}$$

In Eq. (1.4.1) all intermolecular interactions were formally eliminated by introducing the local electric field through

$$\mathbf{E}_L(\mathbf{r}_n, t) = \mathbf{E}(\mathbf{r}_n, t) - \frac{\hbar}{\mu}\sum_m{}' J_{nm}[\langle B_m\rangle + \langle B_m^\dagger\rangle] \tag{1.4.2a}$$

or in k space

$$\mathbf{E}_L(\mathbf{k}, t) \equiv \mathbf{E}(\mathbf{k}, t) - [\hbar J(\mathbf{k})/\mu^2\rho]P(\mathbf{k}, t). \tag{1.4.2b}$$

The nonlocal character of the damping was neglected, and we have set $\Gamma_{nm} = \Gamma\delta_{nm}$. Otherwise, a local picture is impossible. The polarization at every site behaves as an oscillator driven by the local electric field and by anharmonic (nonlinear) forces. The linearized part of Eq. (1.4.1) obtained by neglecting the second term on the r.h.s. will result in our previous expression for the dielectric function (Eq. 1.3.7b).

For optical wave vectors and dipolar interactions in the ($\mathbf{k} \to 0$) limit, $J(\mathbf{k}) = -\frac{4\pi}{3\hbar}\rho\mu^2$ [56]. This gives the Lorentz local field [6,9,10,13]

$$\mathbf{E}_L(\mathbf{k}, t) \equiv \mathbf{E}(\mathbf{k}, t) + \frac{4\pi}{3}\mathbf{P}(\mathbf{k}, t). \tag{1.4.3}$$

In this limit, Eqs. (1.4.1) and (1.4.3) result in the Clausius-Mossotti expression for the dielectric function

$$\frac{\varepsilon(\omega) - 1}{\varepsilon(\omega) + 2} = \frac{4\pi}{3}\rho\alpha(\omega), \tag{1.4.4a}$$

with

$$\alpha(\omega) = \frac{2\Omega\hbar|\mu|^2}{-(\omega + i\Gamma)^2 + \Omega^2}. \tag{1.4.4b}$$

Here $\alpha(\omega)$ is the polarizability of an isolated molecule defined by Eq. (1.3.7a), with $\mathbf{E}_j$ representing the local field, and we have set $\mathbf{k} = 0$.

For subsequent manipulations we further introduce the local-field correction factor

$$S(\mathbf{k}, \omega) \equiv E_L(\mathbf{k}, \omega)/E(\mathbf{k}, \omega). \tag{1.4.5}$$

Combining this with Eq. (1.4.3), we get

$$S(\mathbf{k}, \omega) = \frac{\varepsilon(\mathbf{k}, \omega) + 2}{3}. \tag{1.4.6}$$

A common phenomenological procedure for calculating the nonlinear optical response is based on the cubic-oscillator model [6]. This amounts

to adding a $\sim\mathbf{P}^3$ term in the potential which results in an equation similar to Eq. (1.4.1) but with the second (nonlinear) term in the r.h.s. replaced by $\sim P^2(\mathbf{r}, t)$. Equation (1.4.1) shows that this model is only of limited qualitative value. We find no $\sim P^2$ type of nonlinearity. Instead we have $E_L P^2$, $E_L\dot{P}^2$ and $E_L P\dot{P}$ types of terms. The anharmonicity is thus a function of both the "position" (P) and the "velocity" ($\dot{P}$) of the oscillator as well as the local electric field E_L (5.36].

The single-particle factorization used here leads to a local-field description. Consequently, it is possible to write the susceptibility Eq. (1.3.8) as the third order polarizability of a single molecule $\gamma(-\omega_s; \omega_1, -\omega_2, \omega_3)$ multiplied by local-field correction factors [5,8]

$$\chi^{(3)}(-\mathbf{k}_s - \omega_s; \mathbf{k}_1\omega_1, -\mathbf{k}_2 - \omega_2, \mathbf{k}_3\omega_3)$$
$$= \rho\gamma(-\omega_s; \omega_1, -\omega_2, \omega_3)S(\mathbf{k}_1\omega_1)S(-\mathbf{k}_2 - \omega_2)S(\mathbf{k}_3\omega_3)S(\mathbf{k}_s\omega_s) \tag{1.4.7a}$$

with

$$\gamma(-\omega_s; \omega_1, -\omega_2, \omega_3)$$
$$= 4\Omega\frac{\tilde{\mu}\tilde{\mu}\tilde{\mu}\tilde{\mu}}{\hbar^3}\frac{[-\Omega - \omega_2 + i\Gamma(\mathbf{k}_2)][(\Omega + \omega_1 + i\Gamma(\mathbf{k}_1)]}{[-(\omega_s + i\Gamma)^2 + \Omega^2][-(\omega_1 + i\Gamma)^2) + \Omega^2][-(-\omega_2 + i\Gamma)^2) + \Omega^2]},$$
$$(+\text{permutations of } j = 1, 2, 3], \tag{1.4.7b}$$

and

$$S(\mathbf{k}, \omega) \equiv \frac{-(\omega + i\Gamma)^2 + \Omega^2}{-(\omega + i\Gamma(\mathbf{k}))^2 + \Omega_{\mathbf{k}}^2}. \tag{1.4.7c}$$

The numerators in the $S(\mathbf{k}, \omega)$ factors in Eq. (1.4.7a) cancel the three molecular (Ω) resonances in γ and introduce new exciton ($\Omega_{\mathbf{k}}$) resonances. The permutations of $(\mathbf{k}_1, \omega_1)$, $(-\mathbf{k}_2, -\omega_2)$ and $(\mathbf{k}_3, \omega_3)$ account for the six different time orderings with which the electric fields can interact with the system.

5. THE ROLE OF TWO EXCITON VARIABLES; ENHANCED NONLINEAR SUSCEPTIBILITIES IN MOLECULAR AGGREGATES

In this section we explore the role of the two-exciton variables $\langle B_n B_m\rangle$ in the cooperative enhancement of optical nonlinearities [28]. These variables are particularly important in finite-size systems with restricted geometries such as molecular aggregates or monolayers [26,27,58]. We shall therefore analyze a specific model of confined excitons.

Consider a linear aggregate consisting of N coupled two-level molecules with transition frequency Ω and nearest neighbor dipole–dipole coupling V [28]. N is taken to be odd. The calculation for N even can be made along the same lines and will be omitted here for brevity. The nth molecule is located at $\mathbf{r}_n = n\mathbf{a}$ where $\mathbf{a}$ is the lattice vector, and $\mathbf{r}_{N+1} = \mathbf{r}_1$ (periodic boundary conditions). We further neglect the exciton-phonon coupling. $\chi^{(3)}$ for the present model can be expressed in terms of the single-exciton and two-exciton eigenstates. We shall first introduce these states, which can be exactly calculated for the present model in the Heitler-London approximation, and analyze the resulting $\chi^{(3)}$ obtained using the conventional sum-over-states expression. We then show how these results can be obtained using the present equation of motion approach by simply adopting the factorization (Eq. 1.3.11), which retains only two-exciton variables. We explore the roles of intra and intermolecular nonlinearities, show the limitations of the local-field approximation, and discuss the factors affecting cooperative enhancement. The relevant eigenstates of the aggregate are shown in Fig. 1. They are grouped in three levels. The lowest is the ground state $|g\rangle$. The next level includes N single-exciton states

$$|k\rangle \equiv B_k^\dagger|0\rangle, \tag{1.5.1a}$$

with energies $$\Omega_k \equiv \Omega + 2V\cos\left(\frac{2\pi k}{N}\right), \qquad \mathbf{k} = 0, 1, \ldots, N-1. \tag{1.5.1b}$$

Finally we have the two-exciton manifold

$$|k, q\rangle \equiv C_{k,q}^\dagger|0\rangle, \tag{1.5.2a}$$

with the two-exciton creation operators

$$C_{k,q}^\dagger \equiv \sum_R \sum_s \exp(i2\pi kR/N)\sin\frac{\pi qs}{N} B_{R-s/2}^\dagger B_{R+s/2}^\dagger, \qquad q = 1, 3, \ldots, N-2. \tag{1.5.2b}$$

These operators, when acting on the ground state, create two-exciton states with relative momentum $2\pi q/Na$, center of mass momentum $2\pi k/Na$, and energies

$$\omega_{k,q} = \Omega + 2V\cos\frac{\pi k}{N}\cos\frac{\pi(q-1)}{N}. \tag{1.5.2c}$$

By the Pauli exclusion we have N possibilities for the first excitation and only $N-1$ for the second. There are therefore $N(N-1)/2$ two-exciton states. (The factor 2 results from the permutation of these two excitations). Altogether we need consider $1 + N(N+1)/2$ eigenstates.

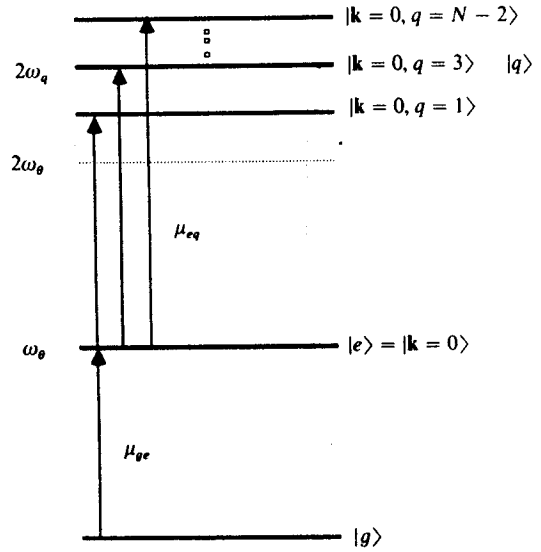

Fig. 1. Energy level diagram for a molecular aggregate, showing the single-photon allowed exciton states and the two-photon allowed two-exciton states. J is taken to be negative (attractive interaction , as in J aggregates) [37] and the exciton-two-exciton splitting $\omega_q - \omega_e$ is therefore positive. In this case strong two-photon absorption will occur to the blue of the exciton resonance.

For simplicity we hereafter specialize to a uniform excitation induced by an external electric field with a wave vector, oriented normal to the aggregate axis, which excites only the $k = 0$ states. We thus need consider only a single-exciton state $|e\rangle \equiv |k = 0\rangle$ and only $(N-1)/2$ two-exciton states $|q\rangle \equiv C_{o,q}^\dagger|0\rangle$. Together with the ground state we have $1 + (N+1)/2$ states. A general analysis for $k \neq 0$ excitons, excited when the aggregate axis not normal to the laser beam wavevector, is straightforward [28]; however, all of the essential physics is contained in the $k = 0$ exciton analysis. We further specialize to a particular $\chi^{(3)}$, which is responsible for nonlinear index of refraction and two-photon absorption of a single beam. Using the standard sum over states expression for $\chi^{(3)}$ [6] we then get

$$\chi^{(3)}(-\omega; \omega, -\omega, \omega) = \rho\frac{1}{(\omega-\omega_e)^2 + (\gamma_e/2)^2}\left[\frac{|\mu_{ge}|^4}{\omega - \omega_e + i\gamma_e/2} - \sum_q \frac{|\mu_{ge}|^2|\mu_{eq}|^2}{2\omega - 2\omega_q + i\gamma_q}\right], \tag{1.5.3}$$

with energies $\omega_e \equiv \Omega + 2V$ and $\omega_q \equiv \omega_e + 2V[\cos(\pi q/N) - 1]$; $q = 1, 3, \ldots, N-2$, γ_e and γ_q are phenomenological relaxation rates of the

exciton and two-exciton states respectively. ρ is the number of aggregates per unit volume. The transition dipole moments are $\mu_{ge} = \sqrt{N}\mu$ and $\mu_{eq} = 2(2\mu/\sqrt{N})\cot(\pi q/2N)$, μ being the transition dipole of a single molecule. They satisfy the sum rule

$$\sum_{q=1,3}^{N-2} |\mu_{eq}|^2 = 2|\mu_{ge}|^2 \frac{N-1}{N}. \tag{1.5.4}$$

$\chi^{(3)}$ is composed of two terms (Liouville-space pathways) [42]. The first term in the square brackets represents the contribution of the single-exciton level and scales as $|\mu_{eg}|^4 \sim N^2$. The second term consists of a series of two-exciton resonances. Using the sum rule (Eq. 1.5.4), the integrated area of these resonances scales as

$$(1/2)|\mu_{ge}|^2 \sum_q |\mu_{eq}|^2 = |\mu|^4 N(N-1).$$

When the laser beams are tuned far from an excitonic or two-excitonic resonance, the two terms intefere destructively, and the N^2 parts exactly cancel out, leaving an overall linear dependent of $\chi^{(3)}$ on size [29,29]

$$\chi^{(3)}(-\omega;\omega,-\omega,\omega) = \rho N|\mu|^4 \frac{1}{(\omega-\omega_e)^2+(\gamma_e/2)^2}\frac{1}{\omega-\omega_e+i\gamma_e/2}. \tag{1.5.5}$$

In small aggregates the exciton and the two-exciton contributions may be well separated spectrally (i.e., $\omega_e - \omega_q$ is larger than the dephasing rates γ_e and γ_q). By carefully tuning the frequency near resonance, it may be possible spectrally to select either the first or the second term of Eq. (1.5.3), resulting in an $\sim N^2$ scaling of the nonlinear response due to cooperative enhancement. An increase in aggregate size N reduces the exciton-two-exciton splitting of the lowest q states, which contain most of the oscillator strength. When that splitting becomes comparable to the exciton linewidth γ, (where γ stands for γ_e or γ_q), it becomes impossible to spectrally select one of these terms. The interference will thus cancel the enhancement, resulting in an $\sim N$ scaling of $\chi^{(3)}$. The crossover size, whereby the magnitude of the aggregate response changes from $\sim N^2$ to $\sim N$, is a solution to $8\sin^2(\pi/2N_c) = \gamma/V$, which gives [28]

$$N_c = \pi[2V/\gamma]^{1/2}. \tag{1.5.6}$$

In summary, the present model provides a simple expression for the nonlinear optical response of aggregates and demonstrates the origin of the crossover from the small aggregate to the bulk limit. Cooperatively enhanced optical nonlinearities ($\sim N^2$) are only possible in small aggregates with

$N < N_c$, where the two-level excitonic resonance is spectrally well separated from the two-photon resonances. In larger aggregates, the intermolecular nonlinearities due to exciton–exciton scattering are diminished, so that the hyperpolarizability is simply proportional to size. This reduction is caused by interference between excitonic nonlinearities and two-photon nonlinearities.

We shall now derive these results directly from our equations of motion, without making summations over eigenstates. This will provide an alternative interpretation for the aggregate size scaling, in terms of anharmonic-oscillators related to intermolecular coherences. Furthermore, the equation of motion result can be easily generalized by a systematic improvement of the factorization, taking into account other important many-body effects. This will be demonstrated in the coming sections. When phonons are neglected, we can make the pure-state ansatz (Eq. 1.3.11). We thus need to consider only the variables $\langle B_n\rangle$ and $\langle B_nB_m\rangle$ and their Hermitian conjugates $\langle B_n^\dagger\rangle$ and $\langle B_n^\dagger B_m^\dagger\rangle$. The equation of motion for $B_n^\dagger B_m^\dagger$ is obtained by substituting these operators in the Heisenberg equation (Eq. 1.3.1), resulting in the following closed equations in momentum space [28]:

$$\frac{d}{dt}\langle B_0^\dagger\rangle = (i\omega_e - \gamma_e/2)\langle B_0^\dagger\rangle + \sum_{q=1,3,\ldots}^{N-2} K(q)\langle C_q^\dagger\rangle\langle B_0\rangle + i\frac{\mu}{\hbar}E(r,t)\left[N - \frac{2}{N}\langle B_0^\dagger\rangle\langle B_0\rangle\right], \tag{1.5.7a}$$

$$\frac{d}{dt}\langle C_q^\dagger\rangle = (2i\omega_q - \gamma_q)\langle C_q^\dagger\rangle + 2i\frac{\mu}{\hbar}E(r,t)\cot\frac{\pi q}{2N}\langle B_0^\dagger\rangle \tag{1.5.7b}$$

with

$$K(q) = \frac{2i}{N^2}\sum_{q'=1,3} 4V\cot\left(\frac{\pi q'}{2N}\right)\left(\cos\frac{\pi q}{N} - 1\right). \tag{1.5.7c}$$

$B_0^\dagger \equiv \sum_0 B_n^\dagger$ represents delocalized single-photon coherences, which, to lowest order in the external electric field, oscillate at the exciton frequency, $\omega_e = \Omega + 2V$. The $(N-1)/2$ two-exciton operators $C_q^\dagger \equiv C_{k=0,q}^\dagger$ represent delocalized two-photon coherences. Equations (1.5.7) imply that calculating the optical nonlinearities requires solving the dynamics of a set of $(N+1)/2$ coupled anharmonic oscillators; a single-exciton oscillator that represents intramolecular coherence and $(N-1)/2$ two-exciton oscillators that represent intermolecular coherences. Equations (1.5.7) can be solved perturbatively in the field E, by expanding $\langle B_0^\dagger\rangle$ and $\langle C_q^\dagger\rangle$ in a Taylor series in E and determining the expansion coefficients order by order. Solving Eqs. (5.7) to third order in E and calculating the polarization yields Eq. (1.5.3). This

shows that the two-exciton oscillators are responsible for the cooperative enhancement of the optical response.

The present anharmonic-oscillator picture offers an alternative interpretation of the cooperative $\sim N^2$ enhancement and the crossover to $\sim N$ scaling discussed earlier. In accordance with the Pauli exclusion principle, a single site cannot be doubly excited, and as a result excitons are not true bosons (or fermions). Linear optical properties can be exactly evaluated using the boson approximation for single excitons [13], but the approximation breaks down for the dynamics of two-excitons and higher excitons, which are vital for the nonlinear optical response, and can therefore be probed via second and higher order nonlinear optical techniques. Spatially confining the exciton enhances the nonbosonic nature and hence the nonlinear susceptibilities (which would vanish if Frenkel excitons were bosons). The combined influence of the Pauli exclusion and excitonic confinement on the third order nonlinear hyperpolarizability results in the cooperative $\sim N^2$ scaling for small sizes and the $\sim N$ scaling for larger sizes where the excitons become more Boson-like.

In order to illustrate the spectroscopic manifestations of the two contributions to Eq. (5.5), let us consider the third order nonlinear absorption coefficient, $W_{\mathrm{TPA}} \equiv \mathrm{Im}\, \chi^{(3)}(-\omega; \omega, -\omega, \omega)$. Since W_{TPA} may change sign, and we wish to display it on a logarithmic scale, we have plotted the following function

$$K(x) \equiv \frac{x}{|x|} \log(1 + |x|) \tag{1.5.8}$$

where $x = W_{\mathrm{TPA}}$, for $|x| \gg 1$, $K = (\mathrm{sign}\ x) \log|x|$ whereas for $|x| \sim 0$ we have $K \sim x$. The $K(x)$ function is thus simply equal to x, if x is small, and it switches over to a logarithmic scale if $|x|$ is sufficiently large. In Fig. 2 we show $K(W_{\mathrm{TPA}})$ as a function of ω for several size aggregates (as indicated in each panel). In the small aggregate region, $\chi^{(3)}(-\omega; \omega, -\omega, \omega)$ reduces, near resonance, to that of a single excitonic two-level system with a transition dipole $N^{1/2}\mu$, with additional two-photon resonances at $2\omega = 2\omega_q$ on the blue side of the spectrum (we have assumed $V < 0$). Positive values of W_{TPA} correspond to two-photon absorption, whereas negative values represent a bleaching of the excitonic line (saturated absorption). As the aggregate size increases, the $q = 1$ resonance moves towards the exciton line and eventually interferes destructively with it. For larger sizes, the destructive interference is complete, resulting in the cancellation of the $\sim N^2$ prefactor in $\chi^{(3)}(-\omega; \omega, -\omega, \omega)$. At this point W_{TPA} scales linearly with N; the red side of the spectrum has converged completely, while the blue side still shows

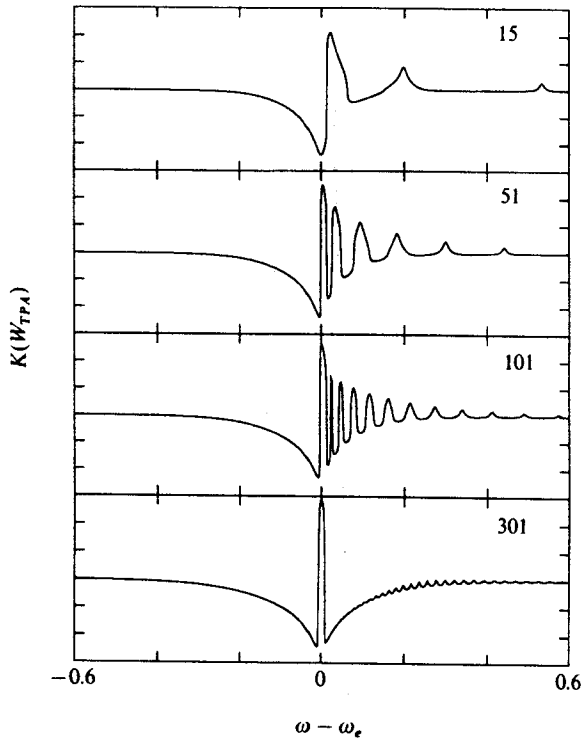

Fig. 2. The nonlinear two-photon absorption calculated using $\chi^{(3)}$ (Eq. 1.5.3). Shown is $K(W_{\mathrm{TPA}})$ where $W_{\mathrm{TPA}} = \mathrm{Im}\, \chi^{(3)}(-\omega; \omega, -\omega, \omega)$ and the function K defined in Eq. (1.5.8). This function displays the signal on a logarithmic scale for large $|W_{\mathrm{TPA}}|$ and on a linear scale for small $|W_{\mathrm{TPA}}|$. Panels show the small aggregate and crossover to the bulk behavior. Note the reduction of the two-exciton blue-shift as the aggregate size is increased. $V = -1$, $\gamma_e = \gamma_q = 0.02$.

resolved two-photon resonances. These, however, becomes more congested as N increases, and eventually the finite experimental spectral resolution will exceed the line spacing, making the blue side a smooth function of $\Delta\omega$, with no N dependence.

In conclusion, we note that the analysis presented in this section and Eq. (1.5.3) constitute a special limiting case of the theory developed in [28b], in which the complete wave vector and frequency dependent susceptibility $\chi^{(3)}(-k_s - \omega_s; k_3\omega_3, k_2\omega_2, k_1\omega_1)$ was calculated. The temperature-dependent superradiant coherence size, which is related to the nonlinear coherence size N_c considered here, was also investigated [37]. It was also shown in [28b] that when $\langle B_n^\dagger B_m^\dagger \rangle$ is factorized into $\langle B_n^\dagger \rangle \langle B_m^\dagger \rangle$, we recover the single-particle

expressions derived in Section 4. In general, when ω is close to the exciton resonance (ω_e), the local-field approximation is inadequate, completely missing the intermolecular nonlinearities; the local-field approximation does not reproduce the correct magnitude of $\chi^{(3)}$. In addition, within this approximation the small aggregate region is completely missed, the N^2 prefactor never appears, and the two-photon resonances are missed [28b].

6. EXCITON-POPULATION VARIABLES AND EXCITON TRANSPORT

In this section, we pursue further our study of nonlinear susceptibilities by adopting the factorization (Eq. 1.3.12) of the three-operator variables,

$$\langle B_n^\dagger B_n B_m \rangle = \langle B_n^\dagger B_n \rangle \langle B_m \rangle \equiv \langle W_n \rangle \langle B_m \rangle. \tag{1.6.1}$$

This factorization is expected to hold in the presence of sufficiently fast phonon-induced dephasing processes that destroy molecular coherences. Using the present factorization we therefore completely neglect intermolecular coherences and miss the cooperative enhancement associated with the two-excitonic variables as discussed in Sec. 5. However, the $\langle W_n \rangle$ variables allow the introduction of exciton transport into the nonlinear response. For the sake of clarity we focus our attention in this section on a specific four-wave mixing technique, degenerate four-wave mixing and its time-domain analogue, and the transient grating [55,22,23]. These techniques are particularly sensitive to the dynamics of the $\langle W_n \rangle$ variables.

6.1. Interaction-Induced Extra Resonances: Degenerate Four-Wave Mixing

Once the factorization (Eq. 1.6.1) is made, we need to derive an equation of motion for the exciton population variables $\langle W_n \rangle$. Instead of doing that, we consider the more general two-particle variables $\langle B_n^\dagger B_m \rangle$. In momentum space we define

$$W(\mathbf{k} - \mathbf{k}') \equiv \frac{1}{N} \sum_m W_m \exp[-i(\mathbf{k} - \mathbf{k}') \cdot \mathbf{r}_m] = \frac{2}{N} \sum_{\mathbf{k}''} B^\dagger_{\mathbf{k}' + \mathbf{k}''} B_{\mathbf{k} + \mathbf{k}''} \tag{1.6.2}$$

and

$$Q(\mathbf{k}, \mathbf{p}, t) \equiv \langle B^\dagger_{\mathbf{p} - \mathbf{k}/2}(t) B_{\mathbf{p} + \mathbf{k}/2}(t) \rangle = \frac{1}{N} \sum_{m,n} \langle B_m^\dagger(t) B_n(t) \rangle \exp[-i\mathbf{k} \cdot (\mathbf{r}_m + \mathbf{r}_n)/2 + i\mathbf{p} \cdot (\mathbf{r}_m - \mathbf{r}_n)], \tag{1.6.3}$$

which are the diagonal elements ($\mathbf{k} = \mathbf{0}$) and coherences ($\mathbf{k} \neq \mathbf{0}$) of the exciton density matrix in the momentum representation. From Eq. (1.6.3), it is clear that $\mathbf{k}$ is conjugate to the exciton center of mass, whereas $\mathbf{p}$ is related to the exciton momentum. The significance of the $\mathbf{k}$ and $\mathbf{p}$ variables may be clarified by switching to the Wigner representation for the exciton density matrix [59,60], which allows us to make the connection to common transport equations such as the Boltzmann equation [61]. This will be illustrated later in this section.

Using Eq. (1.6.1), we obtain the following equations of motion:

$$\frac{1}{i}\frac{d}{dt}\langle B_{\mathbf{k}}(t) \rangle = -(\Omega - i\Gamma(\mathbf{k}))\langle B_{\mathbf{k}}(t) \rangle + \frac{1}{\sqrt{N}} \rho \hbar^{-1} \sum_{\mathbf{k}'} \tilde{\mu} \cdot \mathbf{E}_L(\mathbf{k}', t)[\delta_{\mathbf{k},\mathbf{k}'} - W(\mathbf{k} - \mathbf{k}', t)], \tag{1.6.4a}$$

$$\frac{1}{i}\frac{d}{dt} Q(\mathbf{k}, \mathbf{p}, t) = [J(\mathbf{p} - \mathbf{k}/2) - J(\mathbf{p} + \mathbf{k}/2)]Q(\mathbf{k}, \mathbf{p}, t) - \sum_{\mathbf{p}'} \Sigma(\mathbf{k}; \mathbf{p}, \mathbf{p}')Q(\mathbf{k}, \mathbf{p}', t) - \frac{\sqrt{N}}{\hbar V}(\langle B_{\mathbf{p}+\mathbf{k}/2}(t) \rangle \tilde{\mu} \cdot \mathbf{E}(-\mathbf{p} + \mathbf{k}/2, t) - \langle B^\dagger_{\mathbf{p}-\mathbf{k}/2}(t) \rangle \tilde{\mu} \cdot \mathbf{E}(\mathbf{p} + \mathbf{k}/2, t)), \tag{1.6.4b}$$

$$\mathbf{W}(\mathbf{k}, t) = \frac{2}{N} \sum_{\mathbf{p}} Q(\mathbf{k}, \mathbf{p}, t), \tag{1.6.4c}$$

with V being the quantization volume and the local-field E_L given by Eq. (1.4.2). The first r.h.s. term in Eq. (1.6.4b) describes the free-exciton motion, and the last term represents a source for two-particle coherences created by a combined effect of the electric fields and the polarization. The second r.h.s. term is due to the phonon bath, and $\Sigma(\mathbf{k}; \mathbf{p}, \mathbf{p}')$ is a complex self-energy matrix. Since the factorization Eq. (1.6.1) can be justified only in the presence of fast dephasing, it is essential to introduce phonon-induced relaxation into the present treatment (in contrast to the factorization used in Sec. 5, which is only valid in the absence of dephasing).

The limitations of the local-field approximation are apparent upon a close inspection of Eqs. (1.6.4). In Eqs. (1.6.4a) all intermolecular interactions are lumped into the local field. This is not the case however for Eq. (1.6.4b), where $J(\mathbf{k})$ enters not solely through the field and is responsible for transport processes, which the local-field approximation completely misses!

We shall now simplify the effects of phonons by adopting the following stochastic model for the exciton-phonon coupling (the Haken-Ströbl model) [60,62,63].

$$H_{\text{ex-phon}} = \hbar \sum_n \delta\Omega_n(t) B_n^\dagger B_n. \tag{1.6.5}$$

$\delta\Omega_n(t)$ is a stochastic Gaussian random variable with the following properties:

$$\langle \delta\Omega_n(t) \rangle = 0, \tag{1.6.6a}$$

$$\langle \delta\Omega_n(t)\delta\Omega_m(t) \rangle = \frac{\hat{\Gamma}}{2}\delta(t-t')\delta_{m,n}. \tag{1.6.6b}$$

When the equations of motion are averaged over the stochastic part, we obtain the following relaxation equations [5,60]:

$$\left[\frac{d}{dt}\langle B_m(t)\rangle\right]_{ph} = -\tfrac{1}{2}(\hat{\Gamma}+\gamma)\langle B_m(t)\rangle, \tag{1.6.7a}$$

$$\left[\frac{d}{dt}\langle B_m^\dagger(t)B_n(t)\rangle\right]_{ph} = -\left[\hat{\Gamma}(1-\delta_{nm})+\gamma\right]\langle B_m^\dagger(t)B_n(t)\rangle, \tag{1.6.7b}$$

where $[\cdots]_{ph}$ denotes the phonon contribution. These equations imply for the self-energies [5]

$$\Gamma(\mathbf{k}) = (\hat{\Gamma}+\gamma)/2, \tag{1.6.8a}$$

$$\Sigma(\mathbf{k};\mathbf{p},\mathbf{p}') = -i(\hat{\Gamma}+\gamma)\delta_{pp'} + i\hat{\Gamma}/N. \tag{1.6.8b}$$

The parameters $\hat{\Gamma}$ and γ are taken to be real. $\hat{\Gamma}$ is the pure dephasing rate, and γ represents the population relaxation rate. This model allows for analytical results while still preserving the essential physical aspects related to pure dephasing.

When Eqs. (1.6.4) are transformed to the frequency domain and solved iteratively, we obtain the nonlinear susceptibility $\chi^{(3)}$. For the sake of clarity we shall now restrict our attention to a specific technique: degenerate four-wave mixing (D4WM), which provides a direct probe for the exciton-population variables. This technique uses two incoming fields $\mathbf{k}_1, \mathbf{k}_2$, and the signal is observed at $\mathbf{k}_s = 2\mathbf{k}_1 - \mathbf{k}_2$ and $\omega_s = 2\omega_1 - \omega_2$. The degenerate four-wave mixing (D4WM) techniques studies the signal in the vicinity of $\omega_1 = \omega_2$, looking for a sharp resonance. The signal intensity $R(\mathbf{k}_s, \omega_s)$ is, within the slowly varying amplitude approximation, proportional to $|\chi^{(3)}(-\mathbf{k}_s-\omega_s;\mathbf{k}_1\omega_1,-\mathbf{k}_2-\omega_2,\mathbf{k}_1\omega_1)|^2$. The solution of Eqs. (1.6.4) results in the following expression for $\chi^{(3)}$ relevant for D4WM [5,55]:

$$\begin{aligned}\vec{\chi}^{(3)}&(-\mathbf{k}_s,-\omega_s;\mathbf{k}_1\omega_1,-\mathbf{k}_2-\omega_2,\mathbf{k}_1\omega_1)\\ &= 2\rho\frac{\vec{\mu}\vec{\mu}\vec{\mu}\vec{\mu}}{\hbar^3}\frac{1}{\omega_s-\Omega_{\mathbf{k}_s}+i(\hat{\Gamma}+\gamma)/2}\frac{1}{\omega_1-\Omega_{\mathbf{k}_1}+i(\hat{\Gamma}+\gamma)/2}\frac{1}{\omega_2-\Omega_{\mathbf{k}_2}-i(\hat{\Gamma}+\gamma)/2}\\ &\times\left\{1-\frac{\hat{\Gamma}}{N}\sum_{\mathbf{p}}\left[-i\omega_{12}-iJ(\mathbf{p}-\mathbf{k}_g/2)+iJ(\mathbf{p}+\mathbf{k}_g/2)+\hat{\Gamma}+\gamma\right]^{-1}\right\}^{-1}.\end{aligned} \tag{1.6.9}$$

The $\mathbf{k}_g \equiv \mathbf{k}_1 - \mathbf{k}_2$ is the grating wavevector. This result is the product of the rotating-wave (resonant) part of Eq. (1.4.7), obtained using the single-particle factorization, and a dephasing-induced correction factor given by the curly brackets, which is unity only if $\hat{\Gamma} = 0$. We note that the first three denominators in Eq. (1.6.9) depend on the frequencies ω_1, ω_2, and $\omega_s \equiv 2\omega_1 - \omega_2$ (single- and three-photon resonances) but not on $\omega_{12} \equiv \omega_1 - \omega_2$, which is a two-photon resonance. The only $\omega_1 - \omega_2$ frequency dependence in $R(\mathbf{k}_s, \omega_s)$ that may give a sharp resonance is then contained in the last (dephasing-induced) factor in Eq. (1.6.9), which is completely missed by the single-particle factorization. Three limiting cases are of special interest [5,55].

1. We first consider molecules with arbitrary interactions in the absence of dephasing. For $\hat{\Gamma} = 0$, the Haken-Ströbl model describes coherent exciton motion on the lattice, and from Eq. (1.6.9) it is clear that the D4WM signal exhibits no resonance as a function of ω_{12} in this limit.
2. For noninteracting molecules ($J(\mathbf{k}) = 0$) we find

$$R(\mathbf{k}_s, \omega_s) \propto 1 + \frac{\hat{\Gamma}(\hat{\Gamma}+2\gamma)}{\omega_{12}^2+\gamma^2}. \tag{1.6.10}$$

   This signal has a Lorentzian resonance at $\omega_{12} = 0$, whose width is the inverse of the excited state lifetime. The resonance disappears in the absence of dephasing. These dephasing-induced resonances have been observed by Bloembergen *et al.* [64] in the gase phase and have been denoted PIER4 (pressure induced extra resonances in four-wave mixing). In molecular crystals similar resonances were observed by Hochstrasser *et al.* [65] and have been denoted DICE (dephasing induced coherent emission). The unique and surprising aspect of these resonances is that usually dephasing results in line-broadening associated with the loss of coherence, whereas here it induces new sharp resonances as ω_{12} is varied. This is a consequence of a delicate interference of various terms contributing to $\chi^{(3)}$, which exactly cancel in the absence of dephasing. The addition of dephasing eliminates this cancellation and results in the new resonance [42].
3. We finally discuss the case of finite interactions in the strong dephasing (incoherent or diffusive) limit, defined by $\hat{\Gamma} \gg |J(\mathbf{p}-\mathbf{k}_g/2) - J(\mathbf{p}+\mathbf{k}_g/2)|$ (for all $\mathbf{p}$) and $\hat{\Gamma} \gg \gamma$. In this limit, the Haken-Ströbl model describes diffusive exciton motion, and we have

$$R(\mathbf{k}_s, \omega_s) \propto 1 + \frac{\hat{\Gamma}(\hat{\Gamma}+2\gamma)}{\omega_{12}^2 + [\gamma + (\mathbf{k}_1-\mathbf{k}_2)^2 D_e]^2}, \tag{1.6.11}$$

with the exciton diffusion constant given by

$$D_e \equiv \frac{1}{|\mathbf{k}_g|^2}\frac{1}{\hat{\Gamma}N}\sum_{\mathbf{p}}[J(\mathbf{p}-\mathbf{k}_g/2)-J(\mathbf{p}+\mathbf{k}_g/2)]^2$$
$$=\frac{4}{|\mathbf{k}_1-\mathbf{k}_2|^2}\frac{1}{\hat{\Gamma}}\sum_m J^2(\mathbf{r}_m)\sin^2\left[\frac{(\mathbf{k}_1-\mathbf{k}_2)\cdot\mathbf{r}_m}{2}\right]. \quad (1.6.12)$$

In the incoherent limit the D4WM signal shows a Lorentzian resonance with a width that is the sum of the inverse excited state lifetime (γ) and a contribution from exciton diffusion ($D_e(\mathbf{k}_1-\mathbf{k}_2)^2$). A similar result holds also for a disordered medium [19].

6.2. Exciton Transport in Real Space: The Wigner Representation

Further physical insight into the equation of motion (1.6.4b) for the two-particle coherences $Q(\mathbf{k},\mathbf{p},t)$ can be obtained by making the connection to macroscopic transport equations, such as the Boltzmann equation and the diffusion equation [61]. To this end, we define the Wigner phase-space distribution function $\phi(\mathbf{r},\mathbf{p},t)$ by [5,59,60]

$$\phi(\mathbf{r},\mathbf{p},t)\equiv\frac{1}{\sqrt{N}}\sum_{\mathbf{k}}Q(\mathbf{k},\mathbf{p},t)\exp[i\mathbf{k}\cdot\mathbf{r}]. \quad (1.6.13)$$

The equation of motion (1.6.4b) for the Wigner distribution reads

$$\frac{d}{dt}\phi(\mathbf{r},\mathbf{p},t)=2\sum_{\mathbf{a}}J(\mathbf{a})\sin(\mathbf{p}\cdot\mathbf{a})\phi(\mathbf{r}+\mathbf{a}/2,\mathbf{p},t)$$
$$-\hat{\Gamma}\sum_{\mathbf{p}'}[g(\mathbf{p}')\phi(\mathbf{r},\mathbf{p},t)-g(\mathbf{p})\phi(\mathbf{r},\mathbf{p}',t)]-\gamma\phi(\mathbf{r},\mathbf{p},t), \quad (1.6.14a)$$

with

$$\langle W_n(t)\rangle=\frac{2}{N}\sum_P\phi(\mathbf{r}_n,\mathbf{p},t). \quad (1.6.14b)$$

The first term in Eq. (1.6.14a) describes coherent exciton motion on the lattice. When the interaction is symmetric ($J(\mathbf{r})=J(-\mathbf{r})$) and has a short range, it reduces to $\mathbf{p}/m^*\cdot\vec{\nabla}_{\mathbf{r}}\phi(\mathbf{r},\mathbf{p},t)$ with the effective mass given by $(m^*)^{-1}=(1/d)\sum_n J(r_n)r_n^2$, d being the dimensionality of the system. Here, n runs over the lattice and $r_n\equiv|\mathbf{r}_n|$. The second term in this equation has the form of the BGK strong collision operator in the Boltzmann equation [61], in which collisions occur with rate $\hat{\Gamma}$, and the momentum after each collision is distributed according to the equilibrium momentum distribution $g(\mathbf{p})$. The strong collision operator conserves the number of particles (population); a

population loss with rate γ is described by the last term. If we take $g(\mathbf{p})=1/N$, where N is the number of lattice sites, then Eq. (1.6.14a) is identical to the Haken-Ströbl model. The Haken-Ströbl model is therefore a high-temperature model, as the equilibrium distribution is then uniform over all momenta. Equation (1.6.14a) can also be connected to other standard transport equations (the diffusion and the master equation) [60].

6.3. Transient Grating: The Time-Domain Analogue of Degenerate Four-Wave Mixing

The exciton-population $\langle B_n^\dagger B_n\rangle$ variables can also be probed by an elegant time-domain technique: transient grating (TG) spectroscopy, which may be related to the Fourier transform of the degenerate four-wave mixing [5,22,23]. The following typical setup is considered. At time $t=0$ two short excitation pulses, $(\mathbf{k}_1,\omega_1)$ and $(\mathbf{k}_2,\omega_2)$, crossed with an angle θ, interfere in the sample and create an excitonic grating. The decay of the grating as a result of dephasing and population relaxation is monitored by applying a probe pulse, $(\mathbf{k}_3,\omega_3)$, at $t=\tau$. The observable $R(\tau)$ is the time-integrated intensity of the nonlinear ("diffracted") signal with wave vector $\mathbf{k}_s=\mathbf{k}_1-\mathbf{k}_2+\mathbf{k}_3$ and frequency $\omega_s=\omega_1-\omega_2+\omega_3$ as a function of the pump-probe delay τ. We shall consider now the three cases discussed in section (6.1).

1. In the absence of dephasing, the TG signal never decays.
2. For noninteracting molecules we get
$$R(\tau)=\exp[-2(\gamma+\hat{\Gamma})\tau]. \quad (1.6.15)$$
In the extreme case of $\hat{\Gamma}=0$, no grating decay is observed, apart from the trivial population decay $\exp(-2\gamma t)$. This result is rigorous for all times, and is easily understood: for $\hat{\Gamma}=0$ the initial state created by the incoming pulses is an exact eigenstate of the crystal. Dephasing destroys the grating and contributes to the decay of the signal.
3. We now turn to the opposite limit of strong scattering, $\hat{\Gamma}\gg\gamma$ and $\hat{\Gamma}\gg J$, where the exciton scattering length is much smaller than the grating length scale (diffusive or incoherent motion). The signal intensity is then given by
$$R(\tau)=\exp[-2\gamma\tau-2D_e|\mathbf{k}_1-\mathbf{k}_2|^2\tau]. \quad (1.6.16)$$
The signal decay rate consists of a wavevector-independent contribution due to population relaxation (2γ) and a contribution from the exciton motion, which is proportional to $|\mathbf{k}_1-\mathbf{k}_2|^2$. This is characteristic for diffusive motion [22,23] and leads for small cross angles θ between the

two pump pulses, to a linear relation between the observed decay rate and θ^2. This relation provides a clear experimental distinction between diffusive and coherent exciton motion. In the incoherent limit, an interesting relation exists between the D4WM and TG signals. Namely, the amplitude of the D4WM signal (Eq. 1.6.11) can be obtained by evaluating the Fourier transform of the amplitude of the TG signal (Eq. 1.6.16) at the frequency ω_{12}.

Finally, we emphasize that we have only studied D4WM and the TG within the two-particle description. The single-particle description would lead to exponential decay independent of the magnitude of $\hat{\Gamma}$. Diffusive behavior cannot be found in the single-particle level of description, which is intimately related to the fact that in the single-particle factorization no two-photon ω_{12} resonance is found in the D4WM signal.

7. GREEN FUNCTION EXPRESSIONS FOR $\chi^{(3)}$ IN MOLECULAR NANOSTRUCTURES WITH ARBITRARY GEOMETRY

In the previous sections we have considered separately two important sources of optical nonlinearities. The $\langle B_n^\dagger B_n \rangle$ terms constitute local contributions whereas the two-excitonic variables $\langle B_n^\dagger B_m^\dagger \rangle$ represent nonlocal contributions. Applications were made to periodic assemblies (one-dimensional and three-dimensional). In this section we derive more general equations of motion that allow us to calculate the nonlinear susceptibility $\chi^{(3)}$ of assemblies of molecules with nonoverlapping charge distributions and an arbitrary geometry. The equations incorporate the contribution of all quadratic (bilinear) and cubic exciton variables and include the results of the previous sections as special cases. The equations can be solved using Green function techniques [39]. We provide an explicit solution in the absence of relaxation [66] and present some numerical calculations for one-, two-, and three-dimensional assemblies. We first invoke the Heitler-London approximation where the dipole dipole interaction in Eq. (1.2.2b) is replaced by

$$\frac{\hbar}{2}\sum_{m,n}{}' J(\mathbf{r}_{mn})(B_m^\dagger B_n + B_m B_n^\dagger). \tag{1.7.1}$$

This approximation implies that we work in first-order perturbation theory in the small parameter J/Ω, where J is the interaction energy between

molecules and Ω is the molecular excited-state energy. It allows us to classify the variables by their nonlinear order with respect to the field. (It is possible to develop a perturbation theory and calculate corrections of higher order in J/Ω.) We further introduce the notion of *normal ordering* of operators, *i.e.*, in any product of operators, all $B^\dagger$ are to the left and all B to the right:

$$B_n^\dagger B_m^\dagger \ldots B_{n'} B_{m'} \ldots$$

By using the commutation rules we can bring any product to a normally ordered form. We next note that the expectation value of any normally ordered product of n operators (be it B or $B^\dagger$ must be at least to n'th order in the field. This is the case since initially the density matrix $\rho(0)$ is in the vacuum state. For the sake of evaluating the third-order response, it is thus sufficient to consider only products with up to three B or $B^\dagger$ operators.

Starting with Eq. (1.3.1), we now derive equations of motion for all relevant variables. In addition to the electronic degrees of freedom, we shall incorporate relaxation induced by coupling to nuclear degrees of freedom. We have outlined earlier a model for damping that results in a simple prescription of how to incorporate it in the equations of motion once expectation values are taken. The model depends on two real parameters $\hat{\Gamma}$ and γ. $\hat{\Gamma}$ is the pure dephasing rate, and γ represents the population relaxation rate. We use the notation $\Gamma \equiv \hat{\Gamma} + \gamma$ for the total dephasing rate in the sequel.

$$\left[\frac{d}{dt}\langle B_m^\dagger(t) B_n(t)\rangle\right]_{\text{ph}} = -[\hat{\Gamma}(1-\delta_{nm}) + \gamma]\langle B_m^\dagger(t) B_n(t)\rangle, \tag{1.7.2a}$$

and

$$\left[\frac{d}{dt}\langle B_n^\dagger(t) B_m(t) B_{n'}(t)\rangle\right]_{\text{ph}} = -[\hat{\Gamma}(\tfrac{3}{2} - \delta_{n,m} - \delta_{nn'}) + \tfrac{3}{2}\gamma]\langle B_n^\dagger(t) B_m(t) B_{n'}(t)\rangle. \tag{1.7.2b}$$

We further introduce the notation

$$\zeta_{nm} \equiv 1 - \delta_{nm}.$$

The equations of motion now read

$$\frac{1}{i}\frac{d}{dt}\langle B_n\rangle = \sum_m F_{nm}\langle B_m\rangle + 2\sum_m{}' J_{nm}\langle B_n^\dagger B_n B_m\rangle + \mu_n \frac{E_n(t)}{\hbar}(1 - 2\langle B_n^\dagger B_n\rangle), \tag{1.7.3a}$$

$$\frac{1}{i}\frac{d}{dt}\langle B_n B_m\rangle = \zeta_{nm}\sum_l (F_{n,l}\langle B_l B_m\rangle + F_{m,l}\langle B_n B_l\rangle) + \mu_n\zeta_{nm}\frac{E_n(t)}{\hbar}\langle B_m\rangle + \mu_m\zeta_{nm}\frac{E_m(t)}{\hbar}\langle B_n\rangle, \tag{1.7.3b}$$

$$\frac{1}{i}\frac{d}{dt}\langle B_n^\dagger B_m\rangle = \sum_l (F_{n,l}\langle B_n^\dagger B_l\rangle - F_{n,l}^*\langle B_l^\dagger B_m\rangle) - i\hat{\Gamma}\delta_{nm}\langle B_n^\dagger B_m\rangle$$
$$- \frac{\mu_n E_n^*(t)}{\hbar}\langle B_m\rangle + \frac{\mu_m E_m(t)}{\hbar}\langle B_n^\dagger\rangle, \tag{1.7.3c}$$

$$\frac{1}{i}\frac{d}{dt}\langle B_n^\dagger B_m B_l\rangle = \xi_{ml}\sum_i [F_{m,i}\langle B_n^\dagger B_i B_l\rangle + F_{l,i}\langle B_n^\dagger B_m B_i\rangle$$
$$- F_{n,i}^*\langle B_i^\dagger B_m B_l\rangle] - i\hat{\Gamma}\xi_{ml}(\delta_{nm}+\delta_{nl})\langle B_n^\dagger B_m B_l\rangle$$
$$- \frac{\mu_n E_n^*(t)}{\hbar}\xi_{ml}\langle B_m B_l\rangle + \frac{\mu_m E_m(t)}{\hbar}\zeta_{ml}\langle B_n^\dagger B_l\rangle$$
$$+ \frac{\mu_1 E_1(t)}{\hbar}\zeta_{ml}\langle B_n^\dagger B_m\rangle. \tag{1.7.3d}$$

with

$$F_{nm} \equiv -\Omega_n\delta_{nm} - J_{nm} + i\frac{\Gamma}{2}\delta_{nm}. \tag{1.7.4}$$

The ξ_{nm} factors in these equations result from the Pauli exclusion and guarantee that $\langle B_n B_n\rangle = 0$ at all times (only a single exciton is allowed at a given site). Their presence complicates the solution. Technically it is possible to use a different model in which excitons are bosonlike and omit the ξ factors [39,66]. To account for the Pauli exclusion we then add a repulsive exciton–exciton interaction and change the frequency of $\langle B_n B_m\rangle$ in Eq. (1.7.3b) from $\Omega_n + \Omega_m$ to $\Omega_n + \Omega_m + g$. This model is easier to solve. By sending $g \to \infty$ at the end, we exclude the two exciton states and obtain the solution of Eqs. (1.7.3).

We next introduce the polarization of the nth molecule

$$P_n \equiv \tilde{\mu}(B_n + B_n^\dagger).$$

In order to calculate the linear response we neglect the nonlinear terms in Eq. (1.7.3a), which contribute only to third (and higher) orders in the field, and obtain

$$P_n^{(1)}(\omega) = \sum_m \alpha_{nm}(\omega)E_m(\omega),$$

with the linear polarizability

$$\alpha_{nm}(\omega) = |\mu|^2[G_{nm}(\omega) + G_{nm}^*(-\omega)]. \tag{1.7.5}$$

Here G_{nm} is the single-exciton Green function defined as follows:

$$G(\omega) = (\omega - F + i\eta)^{-1}. \tag{1.7.6}$$

The single-exciton Green function can be evaluated explicitly by introducing the one-exciton wavefunctions $\psi_\alpha(n)$:

$$\Psi_\alpha = \sum_n \psi_\alpha(n)B_n^\dagger|0\rangle, \tag{1.7.7a}$$

which satisfy the equation

$$H_{ex}\Psi_\alpha = \varepsilon_\alpha\Psi_\alpha. \tag{1.7.7b}$$

H_{ex} is given by Eq. (1.2.2b), using the Heitler-London approximation (Eq. (1.7.1)). In the frequency domain we then have

$$G_{nm}(\omega) = \sum_\alpha \frac{\psi_\alpha(n)\psi_\alpha^*(m)}{\omega - \varepsilon_\alpha + i\eta}, \tag{1.7.8}$$

where η is a small positive number that is set to zero at the end of the calculation.

We next turn to the calculation of the third-order nonlinear polarization $\mathbf{P}^{(3)}$. For weak fields, the polarization (and the expectation values of the B_n and $B_n^\dagger$ operators) is small. To find the nonlinear response we can therefore make a perturbative expansion in the number of B factors, provided they are normally ordered. We thus calculate $\langle B_n\rangle^{(1)}$ to first order, then solve for $\langle B_n^\dagger B_m\rangle^{(2)}$, $\langle B_n B_m\rangle^{(2)}$, and finally substitute these back in Eq. (1.7.3a) and solve for $\langle B_n\rangle^{(3)}$.

A Green function solution of Eqs. (1.7.4) was derived in [39] using the factorization (1.3.13). Here we consider the simpler case where relaxation is negligible $\hat{\Gamma} = \gamma = 0$, so that the system is in a pure state at all times, and the bras and the kets can be factorized. $\langle B_n^\dagger B_m\rangle = \langle B_n^\dagger\rangle\langle B_m\rangle$ and $\langle B_n^\dagger B_m B_l\rangle = \langle B_n^\dagger\rangle\langle B_m B_l\rangle$. We then need to solve only Eqs. (1.7.3a) and (1.7.3b). Their Green function solution is [66]:

$$\mathbf{p}_n^{(3)}(\omega_s) = \frac{1}{(2\pi)^2}\int d\omega_1\, d\omega_2\, d\omega_3\, \delta(\omega_s - \omega_1 - \omega_2 - \omega_3)$$
$$\times \sum_{m_1,m_2,m_3} \gamma_{nm_1m_2m_3}(-\omega_s;\omega_1,\omega_2,\omega_3)E_{m_1}(\omega_1)E_{m_2}(\omega_2)E_{m_3}(\omega_3), \tag{1.7.9}$$

with the third order polarizability

$$\gamma_{nm_1m_2m_3}(-\omega_s;\omega_1,\omega_2,\omega_3)$$
$$= |\mu|^4 \frac{1}{6}\sum_p \sum_{n',n''} \{G_{nn'}(\omega_s)G^*_{n'm_3}(-\omega_3)G_{n''m_2}(\omega_2)G_{n''m_1}(\omega_1)\bar{\Gamma}_{n'n''}(\omega_1+\omega_2)$$
$$+ G^*_{nn'}(-\omega_s)G_{n'm_3}(\omega_3)G^*_{n''m_2}(-\omega_2)G^*_{n''m_1}(-\omega_1)\bar{\Gamma}^*_{n'n''}(-\omega_1-\omega_2)\}. \quad (1.7.10)$$

Here $\bar{\Gamma}$ is a two-exciton scattering matrix given by

$$\bar{\Gamma}_{n'n''}(\omega) = -2[\mathscr{F}^{-1}(\omega)]_{n'n''}, \quad (1.7.11a)$$

where the $\mathscr{F}$ matrix is

$$\mathscr{F}_{n'n''}(\omega) \equiv \int \frac{d\omega'}{2\pi i} G_{n''n'}(\omega')G_{n''n'}(\omega-\omega'),$$

or, in terms of the single exciton eigenstates,

$$\mathscr{F}_{n'n''}(\omega) = \sum_{\alpha',\alpha} \frac{\psi_{\alpha'}(n')\psi_\alpha(n')\psi^*_\alpha(n'')\psi^*_\alpha(n'')}{\omega-\varepsilon_{\alpha'}-\varepsilon_\alpha+i\eta}, \quad (1.7.11b)$$

and the p sum is over all six permutations of three pairs (m_1,ω_1), (m_2,ω_2), (m_3,ω_3).

The above Green-function expression holds for a molecular assembly with arbitrary geometry. Nanostructures and superlattices often have a periodic geometry, where these expressions can be simplified further. Consider a periodic system in which the molecules occupy a d-dimensional lattice with lattice constant a. Each lattice site is occupied by a two-level molecule with a transition dipole moment μ.

To make use of the translational symmetry of the problem we recast the Green functions in momentum ($\mathbf{k}$) space. We first perform a d-dimensional Fourier transform of the external field. We thus have

$$E(\mathbf{k},\omega) \equiv \sum_{\mathbf{n}} E(\mathbf{r}_\mathbf{n},\omega)\exp(-i\mathbf{k}\cdot\mathbf{r}_\mathbf{n}),$$

where the wavevector $\mathbf{k}$ [with components k_j $j=1,\ldots,d$] is defined in the first Brillouin Zone $0 \le k_j \le (2\pi)/a$. Similarly we define the Green function

$$G(\mathbf{k},\omega) \equiv \sum_{\mathbf{m}} G_{\mathbf{mn}}(\omega)\exp[-i\mathbf{k}\cdot(\mathbf{r}_\mathbf{m}-\mathbf{r}_\mathbf{n})].$$

In a periodic geometry with $\Omega_n = \Omega$ independent on n, the single exciton states have a well-defined momentum $\mathbf{k}$, *i.e.*, $\alpha = \mathbf{k}$ and energy $\Omega_\mathbf{k}$

$$\left.\begin{aligned}\psi_\alpha(\mathbf{n}) &= \exp(i\mathbf{k}\cdot\mathbf{r}_\mathbf{n}),\\ \Omega_\mathbf{k} &= \Omega + \sum_\mathbf{n}\exp(-i\mathbf{k}\cdot\mathbf{r}_\mathbf{n})J_{\mathbf{n}0}.\end{aligned}\right\} \quad (1.7.12b)$$

We then have:

$$G(\mathbf{k},\omega) = \frac{1}{\omega-\Omega_k+i\eta}. \quad (1.7.13)$$

Eqs. (1.7.5) then yield

$$P^{(1)}(\mathbf{k},\omega) = \chi^{(1)}(\mathbf{k},\omega)E(\mathbf{k},\omega), \quad (1.7.14)$$

with

$$\chi^{(1)}(\mathbf{k},\omega) = -\frac{2\Omega_\mathbf{k}|\mu|^2}{(\omega+i\eta)^2-\Omega_\mathbf{k}^2}. \quad (1.7.15)$$

Eqs. (1.7.9) and (1.7.10) then assume the forms

$$P^{(3)}(\mathbf{k}_s,\omega_s) = \frac{a^{2d}}{(2\pi)^{2(d+1)}}\int d\omega_1\, d\omega_2\, d\omega_3\, d\mathbf{k}_1\, d\mathbf{k}_2\, d\mathbf{k}_3$$
$$\times \delta(\omega_s-\omega_1-\omega_2-\omega_3)\,\delta(\mathbf{k}_s-\mathbf{k}_1-\mathbf{k}_2-\mathbf{k}_3)E(\mathbf{k}_1,\omega_1)$$
$$\times E(\mathbf{k}_2,\omega_2)E(\mathbf{k}_3,\omega_3)\chi^{(3)}(-\mathbf{k}_s,-\omega_s;\mathbf{k}_1\omega_1,\mathbf{k}_2\omega_2,\mathbf{k}_3\omega_3) \quad (1.7.16)$$

$$\chi^{(3)}(-\mathbf{k}_s,-\omega_s;\mathbf{k}_1\omega_1,\mathbf{k}_2\omega_2,\mathbf{k}_3\omega_3) = |\mu|^4\frac{1}{6}\sum_p$$
$$\times \{G(\mathbf{k}_s,\omega_s)\mathbf{G}^*(-\mathbf{k}_3,-\omega_3)G(\mathbf{k}_1,\omega_1)G(\mathbf{k}_2,\omega_2)\bar{\Gamma}(\mathbf{k}_1+\mathbf{k}_2,\omega_1+\omega_2)+$$
$$\times G^*(-\mathbf{k}_s,-\omega_s)G(\mathbf{k}_3,\omega_3)G^*(-\mathbf{k}_1,-\omega_1)G^*(-\mathbf{k}_2,-\omega_2)$$
$$\times \bar{\Gamma}^*(-\mathbf{k}_1-\mathbf{k}_2,-\omega_1-\omega_2)\}. \quad (1.7.17)$$

Here the polarization field has a frequency ω_s and momentum $\mathbf{k}_s$, and

$$\bar{\Gamma}(\mathbf{k},\omega) = -2\left(\frac{2\pi}{a}\right)^d\left[\int d\mathbf{k}_1(\omega-\Omega_{\mathbf{k}_1}-\Omega_{\mathbf{k}-\mathbf{k}_1}+i\eta)^{-1}\right]^{-1}. \quad (1.7.18)$$

In concluding this discussion, let us go back to the local field approximation, where we adopt the factorization (Eq. (1.3.10)) and we therefore need to solve only Eq. (1.7.3a). Consider a homogeneous excitation of an assembly of identical molecules so that $E_n(t) = E(t)$, $\mu_n = \mu$ and $\Omega_n = \Omega$. In this case

we have

$$\psi(t) \equiv \langle B_n(t) \rangle,$$

independent on n.

Eq. (1.7.3a) then assumes the form

$$\frac{1}{i}\frac{d\psi}{dt} = \left(-\Omega - J(k=0) + i\frac{\Gamma}{2}\right)\psi + \mu\frac{E(t)}{\hbar}[1 - 2|\psi|^2] + 2J(k=0)|\psi|^2\psi.$$

This local field equation, which is equivalent to Eq. (1.4.1) [19], is closely related to the Landau-Ginzburg theory of phase transitions and has been used to interpret time-domain four-wave mixing measurements in semiconductor nanostructures [67,68,35].

We shall now present numerical calculations for periodic structures with dipolar interactions. We express energies in units of $J \equiv \mu^2/a^3$. We start with a three-dimensional lattice [39]. In the following calculations we aim for the infinite lattice, and our numerical results use finite lattices with periodic boundary conditions. For the three-dimensional calculations we have taken a $79 \times 79 \times 79$ simple cubic lattice, using the minimal-image convention [69]. We shall focus on two four-wave mixing techniques: The two-photon absorption signal is given by

$$W_{\mathrm{TPA}} = \mathrm{Im}\ \chi^{(3)}_{\mathrm{TPA}}, \tag{1.7.13a}$$

where

$$\chi^{(3)}_{\mathrm{TPA}} \equiv \chi^{(3)}(-\mathbf{k} - \omega; \mathbf{k}\omega, -\mathbf{k} - \omega, \mathbf{k}\omega). \tag{7.13b}$$

The two-exciton contribution to W_{TPA} was already displayed in Fig. 2.

The third harmonic signal is given by

$$W_{\mathrm{THG}} = |\chi^{(3)}_{\mathrm{THG}}|^2, \tag{7.27a}$$

where

$$\chi^{(3)}_{\mathrm{THG}} \equiv \chi^{(3)}(-3\mathbf{k} - 3\omega; \mathbf{k}\omega, \mathbf{k}\omega, \mathbf{k}\omega). \tag{7.28b}$$

The two-photon absorption as well as the third-harmonic generation depend in a trivial way on the isolated-molecule transition frequency Ω. We have taken $\Omega = 10^4/J$ in the following calculations.

We first consider two-photon absorption. There is one resonance for TPA. In Fig. 3 we present the TPA signal in three dimensions. We see that the cooperativity gives a large enhancement of the signal, compared with the local-field approximation even for the quite strong damping $\Gamma/J = 1$, and essentially no shift of the resonance.

We next consider third-harmonic generation (THG). In this case there are two resonances, a single-photon resonance at $\omega = \Omega$ and a three-photon

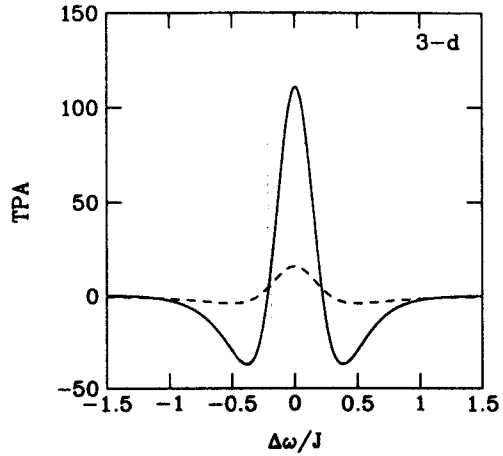

Fig. 3. Two-photon absorption W_{TPA} for a molecular assembly in three W_{TPA} dimensions, $\Delta\omega = \omega - \Omega_s$, at dephasing rate $\Gamma/J = 1, \Omega/J = 10^4$. $\Omega s = \Omega + J(k=0)$ is the single exciton energy. Solid line: numerical results for a $79 \times 79 \times 79$ lattice. Dashed line: local-field approximation, note that $\bar{J} = 0$. The absorption is enhanced by a factor 7 compared with the local field approximation [39].

resonance at $\omega = \Omega/3$. In Fig. 4 we display the THG signal near these two resonances. Note the absence of cooperativity near $\omega = \Omega/3$, where the two-photon levels are nonresonant. In both Figs. 3 and 4, the local-field approximation misses the enhancement entirely.

We next turn to two-dimensional aggregates. We assume that the transition dipole is skewed to the plane at the angle $\theta = 35°$ with $3\cos^2\theta - 1 = 0$, where the one-exciton energy shift vanishes, and the local-field correction vanish. This is intermediate between the H aggregate configuration ($\theta = 90°$) and the J aggregate configuration ($\theta = 0$). The following calculations were made using a square 199×199 lattice. In order to observe directly the deviation from the local-field approximation (cooperative enhancement) we consider a two-color two-photon absorption experiment. We took frequencies such that single-photon transitions are off-resonant, so that we see only the two-photon resonances in the cooperative enhancement factor. The results are displayed in Fig. 5. Notice the complete absence of a resonance in the local-field approximation.

We have further solved Eqs. (1.7.3) approximately for a one-dimensional aggregate with N molecules, using a somewhat different relaxation matrix (this is not essential for the present discussion) [70]. The resulting expression

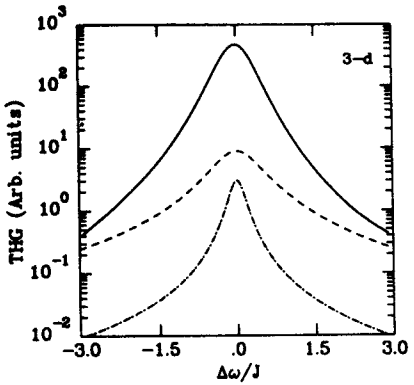

Fig. 4. The third-harmonic signal W_{THG} in three dimensions at dephasing $\Gamma/J = 1$. Solid line: Numerical results for the response near the single-photon resonance Ω_s, $\Delta\omega = \omega - \Omega_s$. Dashed line: local-field result at the same resonance. The enhancement now is 48, the square of the enhancement of the TPA (Fig. 3). The dot-dashed curve shows the three-photon resonance ($\Delta\omega = \omega - \Omega_s/3$). It is actually a superposition of two curves, one dashed, the other dotted corresponding to the numerical solution and the local-field results, respectively. Note the complete absence of enhancement for this resonance [39].

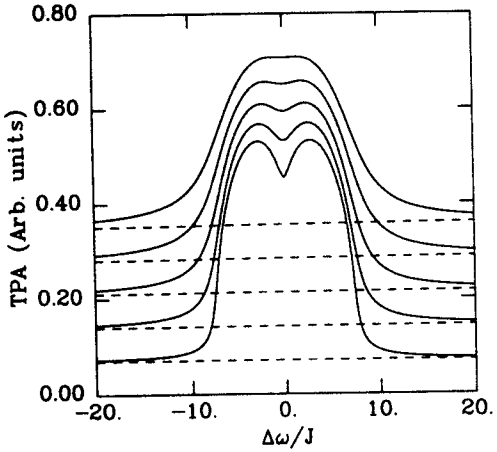

Fig. 5. Two-photon absorption W_{TPA}. The solid lines are numerical results for a two-dimensional assembly at the magic angle for a 199 × 199 lattice, the dashed line is the local-field approximation. Here we have taken $\omega_1 = 0.7\Omega_s + \Delta\omega$, and $\omega_2 = 1.3\Omega_s$. For these frequencies the one-photon frequencies are nonresonant, but the two-exciton term in the cooperativity-enhancement factor is resonant. We have plotted the signal for five dephasing rates, from bottom to top $\Gamma/J = 0.5$, 1, 1.5, 2, and 2.5. The TPA probes the two-exciton resonances which are missed completely by the local-field approximation [39].

for $\chi^{(3)}$ contains the contributions of local as well as nonlocal nonlinearities. The latter may be responsible for an enhanced (cooperative) nonlinear optical response. The enhancement can most conveniently be described in terms of an exciton coherence-size N_c, which represents the separation of two sites that can still respond coherently to the applied fields. In order to define the coherence size more precisely, gain a clear insight into its role, and make the connection with the optical response of aggregates discussed in Sec. 5, we proceed in the following way. We adopt the complete factorization into single operators (Eq. (1.3.10)) if sites n and m are separated by M bonds or more, and the more general factorization (Eq. (1.3.13)) if they are separated by fewer than M bonds. M is a cutoff size that can be varied at will. Nonlocal coherences are important only as long as $|n - m| < N_c$, N_c being the coherence size. We expect $\chi^{(3)}$ to vary with the cutoff M as long as M is smaller than the coherence size N_c. As M exceeds N_c, the factorization (1.3.10) should hold, and $\chi^{(3)}$ should become independent on M. Observing the convergence of $\chi^{(3)}$ as M is varied should provide us with an operational definition of the nonlinear coherence-size N_c.

The present procedure maps the calculation of optical nonlinearities into solving the dynamics of coupled nonlinear oscillators. The oscillators correspond to the single-site variables $\langle B_n \rangle$ and nonlocal variables $\langle B_n B_m \rangle$ and $\langle B_n^\dagger B_m \rangle$, representing molecules separated by fewer than M bonds. In the present picture, the anharmonicities are short-range, and long-range interactions (among molecules separated by more than M bonds) are harmonic and enter only via the local field, which is the field at site n generated by the average field and the contributions of the long-range interactions. Eqs. (1.7.3) then provide a rigorous treatment of short-range dynamics and an approximate mean-field treatment of long-range interactions. The local-field approximation is obtained by taking $M = 1$. In this case, all intermolecular interactions enter via the local field, which, in the long-wavelength limit, it is given by Eq. (1.4.3). As M is increased, we treat the intermolecular interactions more rigorously, and the local field becomes closer to the average field. For $M = N$ we treat all intermolecular interactions explicitly. This interplay among local-field and intermolecular interactions has been discussed by Mukamel, Deng, and Grad[19].

Using the factorization Eq. (1.3.13), $\chi^{(3)}$ has three types of contributions originating from the $\langle B_n^\dagger \rangle \langle B_n \rangle \langle B_m \rangle$, $\langle B_n^\dagger B_m \rangle$, and $\langle B_n B_m \rangle$ nonlinearities. When expanded in powers of molecular density $\rho \equiv 1/a$, we find that the first contribution scales as $\sim\rho$, whereas the second and the third contributions scale as $\sim\rho^2$. This is to be expected, since the first represents the contribution of local nonlinearities whereas the other two are induced by

nonlocal interactions. Nonlocal interactions enter therefore the nonlinear response in two ways; they modify the local term and induce additional terms. The appearance and the form of these new terms provide an excellent direct probe for nonlocal interactions, as was demonstrated in the previous sections.

The following calculations illustrate the relative role of the three types of nonlinearities [70]. In all the calculations we have used nearest neighbor interactions ($J_k = 2V \cos k$) and neglected any explicit dependence on light-wave vectors (the long wavelength approximation) setting $\mathbf{k}_1 = \mathbf{k}_2 = \mathbf{k}_3 = 0$. In Fig. 6 we show the contributions of the cubic and the exciton populations and the two-exciton nonlinearities to the TPA and to the THG signals. $\chi^{(3)}_{\mathrm{THG}}$ is shown in the vicinity of the single-photon resonance $\omega \sim \Omega_0$ and the three-photon resonance $\omega \sim \Omega_0/3$, where $\Omega_0 \equiv \Omega - 2|V|$ is the band-edge frequency. The convergence of $\chi^{(3)}$ with M is shown in Fig. 7.

In our model we have included only exciton repulsion through the Pauli exclusion. Attractive interactions may arise from a variety of sources either direct dipole–dipole interactions or phonon-mediated (very much like the Cooper pairs in superconductivity) [54]. We have calculated the TPA signal and its variation with the phonon-mediated attractive interaction [70]. We

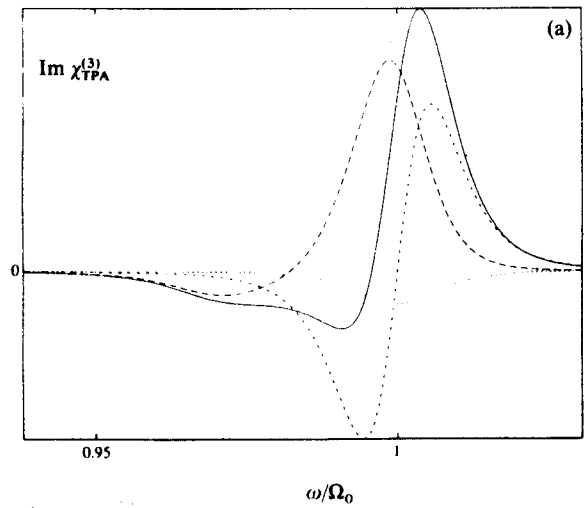

Fig. 6. The contribution of the cubic, exciton population, and two-exciton nonlinearities $\langle B_n^\dagger\rangle\langle B_n\rangle\langle B_m\rangle$, $\langle B_n^\dagger B_m\rangle$ and the $\langle B_n B_m\rangle$ terms in Eq. (1.3.13), to two-photon absorption and third harmonic generation. Solid line—total curve; long dash—two-excitonic contribution; medium dash—exciton population contribution; short dash—cubic nonlinearity contribution. (a) TPA Signal W_{TPA}; (*continued*)

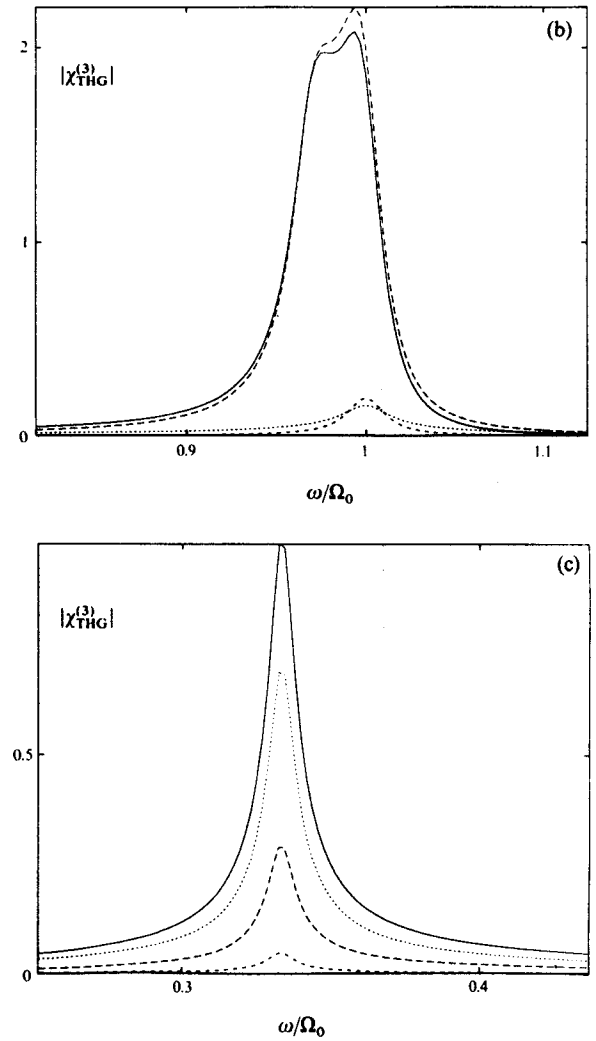

Fig. 6 (*continued*) (b) $|\chi^{(3)}_{\mathrm{THG}}|$, square root of the THG signal in the vicinity of the band edge; (c) $|\chi^{(3)}_{\mathrm{THG}}|$ in the vicinity of the three-photon resonances $\omega \sim \Omega_0/3$ [70].

found a progression of two-photon resonances in the two-exciton band. These resonances are blue-shifted compared with the band edge ($\omega > \Omega_0$). The blue shift results from the Pauli exclusion, which acts as an effective repulsion among excitons. These resonances are very similar to those displayed in Fig. 2. In addition, we noticed the appearance of strong resonances that are red-shifted with respect to the exciton frequency

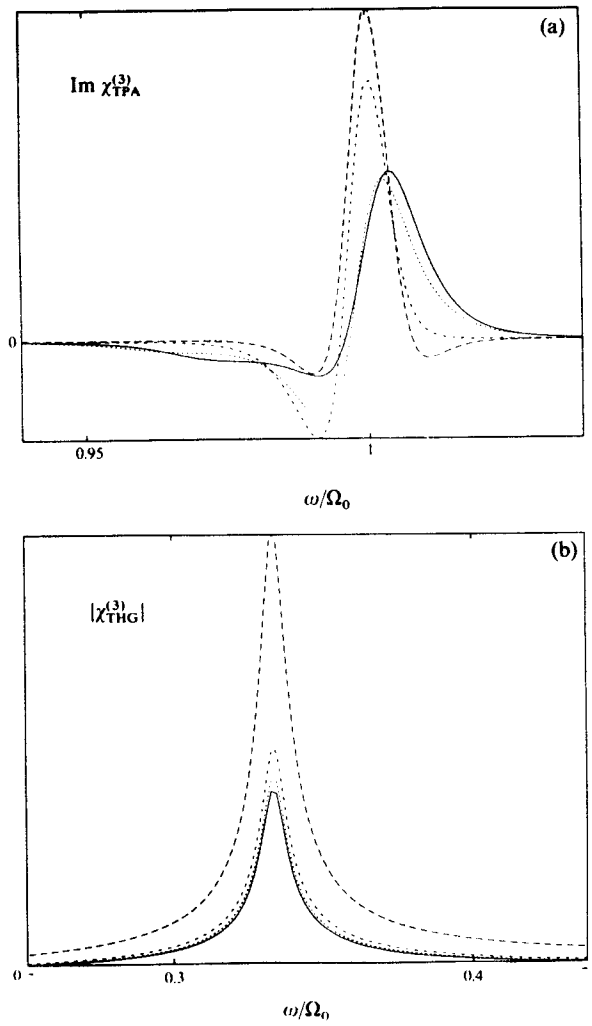

Fig. 7. Dependence of the nonlinear susceptibilities on the truncation size M, for an infinite chain $N \to \infty$ demonstrating the coherence size. (a) TPA signal Im $\chi^{(3)}_{TPA}$. Solid—$M = N$; long dash—$M = 1$; medium dash—$M = 3$; short dash— $M = 6$. (b) Square root of the THG signal $|\chi^{(3)}_{THG}|$ in the vicinity of the three-photon resonance. Solid line—$M = N$; long dash—$M = 1$; medium dash—$M = 2$; short dash—$M = 3$. (*Continued.*)

($\omega < \Omega_0$) and are induced by the attractive interactions. When the attractive part is sufficiently strong a new bound (biexciton) state can be formed, and the red shift is equal to the biexciton binding energy, and it naturally increases with the binding energy.

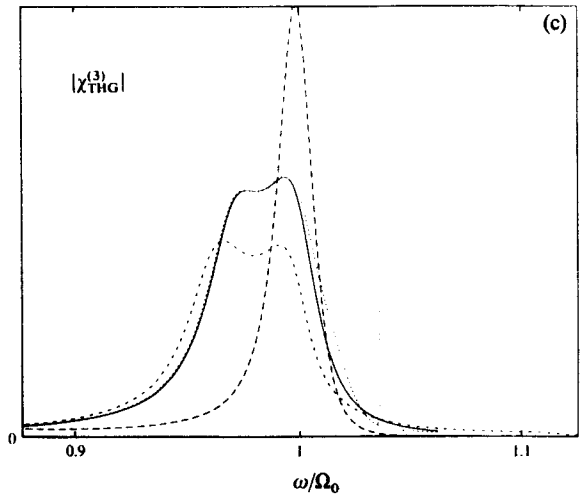

Fig. 7 (*continued*). (c) $|\chi^{(3)}_{THG}|$ in the vicinity of the band edge. Solid line—$M = N$; long dash—$M = 1$; medium dash—$M = 6$; short dash—$M = 12$ [70].

8. DISCUSSION

In this article we have presented a systematic unified methodology for calculating and interpreting the macroscopic nonlinear optical response of molecular materials. We have demonstrated a few manifestations of cooperativity that is totally missed by the local-field approximation. Cooperativity arises from the existence of non-local coherences and is the source of new resonances and possible enhancements (unusually large nonlinearities) as well as other phenomena. Enhanced radiative decay (superradiance) is another manifestation of cooperative radiative dynamics. Superradiance in molecular assemblies was calculated and observed recently [37,38]. The intermolecular nature of the nonlinear response is also reflected in exciton-transport whose signature is the wavevector dependence of $\chi^{(3)}$ and can be probed in the frequency domain (degenerate four-wave mixing) or in the time domain (transient grating spectroscopy).

When all frequencies are tuned far off resonance, the optical response is instantaneous (by the Heisenberg uncertainty, the process is completed in a time scale $\tau \sim \hbar/\Delta E$ with ΔE being an average detuning). Intermolecular interactions then do not have enough time to be effective and may be neglected. The optical response of a molecular material thus reduces to essentially that of a single molecule with minor local-field corrections. The local-field approximation fails completely to take into account any contribu-

tion of non-local nonlinearities. It therefore misses the cooperative effects, and exciton transport. In the design of optical materials it is important to optimize the detunings such that they are sufficiently large to avoid absorptive losses, but sufficiently small to make use of the cooperative effects. The present theory may be helpful in predicting the macroscopic nonlinearities based on individual molecular properties.

The approach developed here establishes an anharmonic-oscillator picture for the nonlinear medium. The linear optical properties in condensed phases can be calculated using a harmonic (Drude) oscillator picture. The optical polarization of a crystal of N two-level atoms is rigorously given by a sum of N coupled harmonic oscillators representing the individual molecular polarizations [10,11,13]. A natural extension of these ideas to nonlinear optics suggests the use of an anharmonic oscillator picture for the material polarization. This model proposed by Bloembergen [6] offers a simple qualitative physical picture, but was never rigorously established. The theory presented here is based upon a microscopic derivation of equations of motion for the optical polarization and other relevant dynamical variables, which are nonlocal in space and represent intermolecular coherences. These variables constitute a set of coupled anharmonic oscillators. The complex many-body problem thus reduces to the coupled nonlinear dynamics of relatively few oscillators. The common procedure, which is routinely used in the calculation of optical nonlinearities of atomic and molecular systems, is based on an expansion of the system's density matrix to third order in the applied fields. This results in a time-ordered expression for $\chi^{(3)}$ in which we keep track of the relative order in time of the interactions with the various electromagnetic fields [6,7,42] as given by the various Liouville-space pathways. When our results are compared with the density matrix time-ordered approach [28], we find the anharmonic-oscillator picture to yield a more compact expression that is much simpler to evaluate since it does not require calculating the molecular eigenstates.

The relevant anharmonic oscillators are identified as follows. We start with the optical polarization which is related to the exciton amplitudes $\langle B_m \rangle$. Its equation of motion couples it to additional variables, which in turn are coupled to more variables. In the present calculations the additional variables include the two-exciton $\langle B_n B_m \rangle$ and the exciton-population and coherence $\langle B_n^\dagger B_m \rangle$ variables. These variables together with their hermitian conjugates constitute the relevant set of anharmonic oscillators.

In this chapter we have applied this procedure for molecular crystals with Frenkel excitons and explored and compared various levels of description. The same procedure can be applied to materials other than molecular

crystals, e.g., semiconductors [36,71], conjugated polyenes [72–75], and the like. The nature of the additional oscillators is going to be different for different materials. Semiconductors and molecular systems with extended (delocalized) electronic states constitute an important class of materials with interesting nonlinear optical properties. Extensive studies have been made on conjugated polymers such as polydiacetylene, polyacetylene, or polysilane. Resonant $\chi^{(3)}$ spectroscopies such as transient grating, optical stark, and coherent Raman reveal useful information regarding the nature of the excitons in these systems. Our reduced equations of motion developed for Frenkel (molecular) excitons may be extended to Wannier excitons by treating the electrons and the holes separately, using two-particle (electron-hole) variables [36,72].

It has been argued that as far as the magnitude of optical nonlinearities are concerned, there is no difference between different materials (molecular, semiconductor, or conjugated systems) [31]. This statement may hold some truth at the single-exciton level, but is clearly an oversimplification, since the nature of higher order variables is very different for various materials. The differences between materials can be very clearly identified and investigated by analyzing the nature of the nonlinear oscillators in each case. These physical differences are much less transparent when using the sum-over-states expression, which is formally the same for all materials, and whereby the differences enter through the complete set of eigenstates. The modelling of optical materials in terms of coupled anharmonic oscillators offers a simple and physically transparent picture that is a natural extension of the harmonic oscillator picture of linear optics. The incorporation of additional (*e.g.*, phonon) degrees of freedom in this picture may be carried out very easily. In the applications presented here, phonons simply result in relaxation and damping of the electronic degrees of freedom. Phonons can sometimes show up as explicit new resonances (rather than broadening). Raman and optical Stark effects are examples [36,71,76,77]. Such measurements can be described by adding more oscillator variables representing phonons in the equations of motion.

The present approach may be applied to various systems with restricted geometries (quantum wells, wires, and dots) where the non-Boson nature of the elementary excitations is amplified. Enhanced nonlinear susceptibilities have been reported in small semiconductor microcrystallites in glasses and polymers due to exciton confinement [34]. The systematic incorporation of disorder in nonlinear susceptibilities constitutes another important open problem in nonlinear optics. Many of the interesting optical materials are disordered. Dye-doped polymers [78] and glasses, mixed monolayers [79],

and concentrated dye solutions are a few examples. There is extensive literature related to the effects of disorder in linear optics and the dielectric function $\varepsilon(\mathbf{k}, \omega)$ [14,15]. The equations of motion and Green function approach is ideally suited for incorporating the effects of disorder including static (substitutional) disorder as well as dynamical disorder (orientational, dielectric relaxation, and the like). An extension to second-order nonlinearities ($\chi^{(2)}$) in organized media such as Langmuir Blodgett films and multilayers is also possible [1]. Ultrafast time-domain spectroscopy with up to femtosecond resolution often provides invaluable information that is complementary to the frequency-domain susceptibilities [42]. The equation-of-motion approach naturally provides the necessary time-domain response functions, which are being probed by these techniques. The factors affecting the switching time scales can be analyzed. Finally, in highly ordered low-temperature materials with a large oscillator strength per unit volume, the radiation field combines with the material polarization to form new elementary excitations: polaritons. Polariton effects in optical nonlinearities, which were not covered here, include a significant change in damping and unusually fast transport rates [23,49]. The present methodology can be extended to incorporate polariton effects [5,50]. The anharmonic oscillators are then combined material and field degree of freedom (rather than purely material variables).

ACKNOWLEDGMENTS

The support of the Air Force Office of Scientific Research, the National Science Foundation, and the Center for Photoinduced Charge Transfer is gratefully acknowledged. I wish to thank my coworkers, in particular J. A. Leegwater, V. Chernyak, J. Knoester, F. C. Spano, O. Dubovsky, H. X. Wang, N. Wang and W. Bosma, who were instrumental in the developments covered in this review.

REFERENCES

1. D. S. Chemla and J. Zyss, *Nonlinear Optical Properties of Organic Molecules and Crystals*, Vols. I and II. Academic, New York, 1987.
2. D. J. Williams, *Nonlinear Optical Properties of Organic and Polymeric Materials.* ACS Symposium, Series 233, Washington, 1983.
3. D. Bedeaux and N. Bloembergen, *Physica* **69**, 67 (1973).
4. H. Haug, ed., *Optical Nonlinearities and Instabilities In Semiconductors.* Academic Press, New York, 1988; H. Haug and S. W. Koch, *Quantum Theory of the Optical and Electronic Properties of Semiconductors.* World Scientific, Singapore, 1990.
5. J. Knoester and S. Mukamel, *Physics, Reports* **205**, 1 (1991).

6. N. Bloembergen, *Nonlinear Optics.* Benjamin, New York, 1965.
7. P. N. Butcher, *Nonlinear Optical Phenomena.* Ohio University Press, Athens, Ohio, 1965.
8. C. Flytzanis, in *Quantum Electronics.* (H. Rabin and C. L. Tang, eds.). Vol. 1, p. 1, Academic Press, New York, 1975.
9. Y. R. Shen, *The Principles of Nonlinear Optics.* Wiley, New York, 1984.
10. H. A. Lorentz, *The Theory of Electrons.* Dover, New York, 1952.
11. M. Born and K. Huang, *Dynamical Theory of Crystal Lattices.* Oxford, London, 1954.
12. P. Mazur, *Adv. Chem. Phys.* **1**, 309 (1958); J. deGoede and P. Mazur, *Physica* **58**, 568 (1972); S. R. DeGroot, *The Maxwell Equations*, North Holland, Amsterdam, 1969.
13. U. Fano, *Phys. Rev.* **103**, 1202 (1956); S. I. Pekar, *Sov. Phys. JETP* **6**, 785 (1958); *ibid.* **11**, 1286 (1960).
14. C. J. F. Bottcher, *Theory of Electric Polarization*, Vol. I, Elsevier, Amsterdam, 1973; C. J. F. Bottcher and P. Bordewijk, *Theory of Electric Polarization*, Vol. II, Elsevier, Amsterdam, 1978.
15. J. Van Kranendonk and J. E. Sipe, in *Process in Optics* (E. Wolf, ed.). Vol. 15, p. 245. North-Holland, Amsterdam, 1977; P. Madden and D. Kivelson, *Adv. Chem. Phys.* **56**, 467 (1984).
16. G. R. Meredith, *J. Chem. Phys.* **75**, 4317 (1981); *ibid.* **77**, 5863 (1982); *Phys. Rev. B* **24**, 5522 (1981).
17. M. Hurst and R. W. Munn, *J. Mol. Elect* **3**, 75 (1987).
18. J. Knoester and S. Mukamel, *Phys. Rev. A* **39**, 1899 (1989); J. Knoester and S. Mukamel, *Phys. Rev. A* **41**, 3812 (1990).
19. S. Mukamel, Z. Deng, and J. Grad, *J. Opt. Soc. Am. B* **5**, 804 (1988).
20. Th. Förster, *Ann. Phys.* (Leipzig) **2**, 55 (1948); D. L. Dexter, *J. Chem. Phys.* **21**, 836 (1953).
21. V. M. Agranovich and M. D. Galanin, in *Electronic Excitation Energy Transfer in Condensed Matter* (V. M. Agranovich and A. A. Maradudin, eds.). North-Holland, Amsterdam, 1982.
22. H. J. Eichler, P. Günter, and D. W. Pohl, *Laser-Induced Dynamic Gratings.* Springer, Berlin, 1986.
23. J. R. Salcedo, A. E. Siegman, D. D. Dlott, and M. D. Fayer, *Phys. Rev. Lett.* **41**, 131 (1978); T. S. Rose, R. Righini, and M. D. Fayer, *Chem. Phys. Lett.* **106**, 13 (1984).
24. G. Roberts, ed. *Langmuir-Blodgett Films.* Plenum, New York, 1990.
25. D. Mobius and H. Kuhn, *Isr. J. Chem.* 18, 375 (1979); D. Mobius and H. Kuhn, *J. Appl. Phys.* **64**, 5138 (1988).
26. F. F. So, S. R. Forrest, Y. Q. Shi, and W. H. Steier, *Appl. Phys. Lett.* **56**, 674 (1990).
27. E. Hanamura, *Phys. Rev. B* **37**, 1273 (1988); *Phys. Rev. B* **38**, 1228 (1988).
28. (a) F. C. Spano and S. Mukamel, *Phys. Rev. A* **40**, 5783 (1989); (b) F. C. Spano and S. Mukamel, *Phys. Rev. Lett.* **66**, 1197 (1991); F. C. Spano and S. Mukamel, *J. Chem. Phys.* **95**, 7526 (1991).

29. H. Ishihara and K. Cho, *Phys. Rev. B* **42**, 1724 (1990); H. Ishihara and K. Cho, *Nonlin. Opt.* **1**, 287 (1992).
30. J. Feldmann, G. Peter, E. O. Gobel, P. Dawson, K. Moore, C. Foxton, and R. J. Elliot, *Phys. Rev. Lett.* **59**, 2337 (1987); F. C. Spano, J. R. Kuklinski, and S. Mukamel, *J. Chem. Phys.* **94**, 7534 (1991).
31. B. I. Greene, J. Orenstein, R. R. Millard, and L. R. Williams, *Phys. Rev. Lett.* **58**, 2750 (1987); B. I. Greene, J. Orenstein; and S. Schmitt-Rink, *Science* **247**, 679 (1990).
32. G. J. Blanchard and J. P. Heritage, *Chem. Phys. Lett.* **177**, 287 (1991); P. D. Townsend, W.-S. Fann, S. Etemad, G. L. Baker, Z. G. Soos, and P. C. M. McWilliams, *Chem. Phys. Lett.* **180**, 485 (1991); S. Etemad and Z. G. Soos, in *Spectroscopy of Advanced Materials* (R. J. H. Clark and R. E. Hester, eds.), p. 87, Wiley, New York, 1991.
33. G. J. Blanchard and J. P. Heritage, *Chem. Phys. Lett.* **177**, 287 (1991); W.-S. Fann, S. Benson, J. M. J. Madey, S. Etemad, G. L. Baker, and F. Kajzar, *Phys. Rev. Lett.* **62**, 1492 (1989).
34. M. G. Bawendi, M. L. Steigerwald, and L. E. Brus, *Ann. Rev. Phys. Chem.* **41**, 477 (1990).
35. S. Schmitt-Rink, D. S. Chemla, and D. A. B. Miller, *Phys. Rev. B* **32**, 6601 (1985); K. Leo, M. Wegener, J. Shah, D. S. Chemla, E. O. Göbel, T. C. Damen, S. Schmitt-Rink, and W. Shäfer, *Phys. Rev. Lett* **65**, 1340 (1990).
36. J. R. Kuklinski and S. Mukamel, *Phys. Rev. B* **42**, 2959 (1990); J. R. Kuklinski and S. Mukamel, *Phys. Rev. B* **42**, 295 (1990); *ibid.* **44**, 253 (1991).
37. J. Grad, G. Hernandez, and S. Mukamel, *Phys. Rev. A* **37**, 3835 (1988); F. C. Spano and S. Mukamel, *J. Chem. Phys.* **91**, 683 (1989); F. C. Spano, J. R. Kuklinski, and S. Mukamel, *Phys. Rev. Lett.* **65**, 211 (1990); F. C. Spano, J. R. Kuklinski, and S. Mukamel, *J. Chem. Phys.* **94**, 7534 (1991); F. C. Spano, J. R. Kuklinski, S. Mukamel, D. V. Brumbaugh, M. Burberry, and A. A. Muenter, *Molecular Crystals and Liquid Crystals* **194**, 331 (1991).
38. S. DeBoer, K. J. Vink, and D. A. Wiersma, *Chem. Phys. Lett.* **137**, 99 (1987); S. DeBoer and D. A. Wiersma, *Chem. Phys. Lett.* **165**, 45 (1990).
39. J. A. Leegwater and S. Mukamel, *Phys. Rev. A* **46**, 452 (1992).
40. P. N. Prasad, E. Perrin, and M. Samoc, *J. Chem. Phys.* **91**, 2360 (1989).
41. R. W. Hellwarth, *Prog. Quantum Electron.* **5**, 1 (1977).
42. S. Mukamel and R. F. Loring, *J. Opt. Soc. Am. B* **3**, 595 (1986); S. Mukamel, *Adv. Chem. Phys.* **70**, Part I, 165 (1988); S. Mukamel, *Ann. Rev. Phys. Chem.* **41**, 647 (1990).
43. M. Gross and S. Haroche, *Phys. Rep.* **93**, 301 (1982).
44. T. Itoh, T. Ikehara, and Y. Iwabuchi, *J. Lumin.* **45**, 29 (1990); T. Itoh and M. Furumiya, *J. Lumin.* **48** and **49**, 704 (1991); T. Itoh, *Nonlinear Optics* **1**, 61 (1991).
45. K. Kemnitz, K. Yoshihara, and T. Tani, *J. Phys. Chem.* **94**, 3099 (1990).
46. J. J. Hopfield and D. G. Thomas, *Phys. Rev.* **132**, 563 (1963); J. J. Hopfield, *Phys. Rev.* **112**, 1555 (1958); *ibid.* **182**, 945 (1969); V. M. Agranovich, *Zh. Eksp. Teor. Fiz.* **37**, 430 (1959) [Sov. Phys.-JETP **37**, 307 (1960)].

47. G. M. Gale, F. Vallée, and C. Flytzanis, *Phys. Rev. Lett.* **57**, 1867 (1986).
48. D. Frölich, S. Kirchhoff, P. Köhler, and W. Nieswand, *Phys. Rev. B* **40**, 1976 (1989).
49. C. K. Johnson and G. J. Small, in *Excited States* (E. C. Lim, ed.), Vol. 6, Academic Press, New York, 1982; S. H. Stevenson, M. A. Connolly, and G. J. Small, *Chem. Phys.* **128**, 157 (1988).
50. J. Knoester and S. Mukamel, *J. Chem. Phys.* **91**, 989 (1989); J. Knoester and S. Mukamel, *Phys. Rev. A* **40**, 7065 (1989).
51. A. S. Davydov, *Theory of Molecular Excitons*, Plenum, New York, 1971.
52. E. I. Rashba and M. D. Sturge, eds., *Excitons.* North-Holland, Amsterdam, 1982.
53. L. N. Ovander, *Usp. Fiz. Nauk* **86**, 3 (1965) [Sov. Phys.-Usp. **8**, 337 (1865)].
54. G. D. Mahan, *Many Particle Physics.* Plenum, New York, 1990.
55. R. F. Loring and S. Mukamel, *J. Chem. Phys.* **84**, 1228 (1986).
56. W. R. Heller and A. Marcus, *Phys. Rev.* **84**, 809 (1951).
57. M. Orrit and P. Kottis, *Adv. Chem. Phys.* **74**, 1 (1988).
58. F. C. Spano, V. M. Agranovich, and S. Mukamel, *J. Chem. Phys.* **95**, 1400 (1991).
59. E. Wigner, *Phys. Rev.* **40**, 749, (1932); M. Hillery, R. F. O'Connell, M. O. Scully, and E. P. Wigner, *Phys. Rept.* **106**, 121 (1984).
60. R. F. Loring, D. S. Franchi, and S. Mukamel, *Phys. Rev. B* **37**, 1874 (1988); S. Mukamel, D. S. Franchi, and R. F. Loring, *Chem. Phys.* **128**, 99 (1988).
61. H. Risken, *The Fokker-Planck Equation.* Springer, Berlin, 1984.
62. H. Haken and G. Strobl, *Z. Phys.* **262**, 135 (1973).
63. D. K. Garrity and J. L. Skinner, *J. Chem. Phys.* **82**, 260 (1985).
64. N. Bloembergen, H. Lotem, and R. T. Lynch, *Indian J. Pure Appl. Phys.* **16**, 151 (1978); Y. Prior, A. R. Bogdan, M. Dagenais, and N. Bloembergen, *Phys. Rev. Lett.* **46**, 111 (1981); L. Rothberg in *Prog. in Optics* (E. Wolf, ed.), Vol. 24, p. 38, North Holland, 1987.
65. J. R. Andrews, R. M. Hochstrasser, and H. R. Trommsdorff, *Chem. Phys.* **62**, 87 (1981); J. R. Andrews, and R. M. Hochstrasser, *Chem. Phys. Lett.* **82**, 381 (1981).
66. V. Chernyak and S. Mukamel, *Phys. Rev. B* (1993, in press).
67. W. Wegener, D. S. Chemla, S. Schmitt-Rink, and W. Schäfer, *Phys. Rev. A* **42**, 5675 (1990).
68. S. Schmitt-Rink and S. Mukamel; K. Leo and J. Shah, and D. S. Chemla, *Phys. Rev. A* **44**, 2124 (1991).
69. M. P. Allen and D. J. Tildesley, *Computer Simulations of Liquids*, Clarendon, Oxford 1987.
70. O. Dubovsky and S. Mukamel, *J. Chem. Phys.* **95**, 7828 (1991); O. Dubovsky and S. Mukamel, *J. Chem. Phys.* **96**, 9201 (1992).
71. S. Schmitt-Rink, D. S. Chemla, and D. A. B. Miller, *Adv. in Physics* **38**, 89 (1989).
72. A. Takahashi and S. Mukamel (to be published); M. Hartmann and S. Mukamel, *J. Chem. Phys.* **99** (in press).
73. A. F. Garito, J. R. Heflin, F. Y. Wong, and Q. Zamani-Khamiri, in *Organic Materials for Nonlinear Optics*, R. A. Hann and D. Bloor (eds.) (Royal Society

of Chemistry, London, 1988), Special Publication No. 69; J. R. Heflin, K. Y. Wong, O. Zamani-Khamiri, and A. F. Garito, *Phys. Rev. B* **38**, 1573 (1988).
74. S. Etemad and Z. G. Soos, in *Spectroscopy of Advanced Materials*, R. J. H. Clark and R. E. Hester (eds.), Wiley, New York (1991); S. N. Dixit, D. D. Guo, and S. Mazumdar, *Mol. Cryst. Liq. Cryst.* **194**, 33 (1991).
75. C. P. deMelo and R. Silbey, *Chem. Phys. Lett.* **140**, 537 (1987); D. Yaron and R. Silbey, *Phys. Rev. B* **45**, 11655 (1992).
76. W. B. Bosma, S. Mukamel, B. I. Greene, and S. Schmitt-Rink, *Phys. Rev. Lett.* **68**, 2456 (1992).
77. R. Zimmermann, *Phys. Stat. Sol. (b)* **159**, 317 (1990); R. Zimmermann and M. Hartmann, *J. Crystal Growth* **101**, 341 (1990).
78. S. Saikan, T. Kishda, Y. Kanematsu, H. Aota, A. Harada, and M. Kamachi, *Chem. Phys. Lett.* **166**, 358, (1990); S. Saikan, A. Imaoka, Y. Kanematsu, K. Sakoda, K. Kominami, and Iwamoto, *Phys. Rev. B* **41**, 3185 (1990).
79. D. Lupo, W. Prass, U. Scheunemann, A. Laschewsky, H. Ringsdorff, and I. Ledeoux, *J. Opt. Soc. Am. B* **5**, 300 (1988); J. S. Schildkraut, T. L. Penner, C. S. Willand, and A. Ulman, *Opt. Lett.* **13**, 134 (1988); L. M. Hayden, *Phys. Rev. B* **38**, 3718 (1988).